

THESIS FOR THE DEGREE OF LICENTIATE OF ENGINEERING

**Simulation studies of new observing concepts for  
geodetic Very Long Baseline Interferometry**

GRZEGORZ KLOPOTEK



**CHALMERS**  
UNIVERSITY OF TECHNOLOGY

DEPARTMENT OF SPACE, EARTH AND ENVIRONMENT  
CHALMERS UNIVERSITY OF TECHNOLOGY  
GOTHENBURG, SWEDEN 2017

## **Simulation studies of new observing concepts for geodetic Very Long Base-line Interferometry**

GRZEGORZ KLOPOTEK

© Grzegorz Klopotek, 2017

Space Geodesy and Geodynamics Group  
Department of Space, Earth and Environment  
Chalmers University of Technology  
SE-412 96 Gothenburg, Sweden  
Phone: +46 (0)31-772 10 00

### **Contact information:**

Grzegorz Klopotek  
Chalmers University of Technology  
Onsala Space Observatory  
SE-439 92 Råö, Sweden

Phone: +46 (0)31-772 55 75  
Email: [grzegorz.klopotek@chalmers.se](mailto:grzegorz.klopotek@chalmers.se)

### **Cover image:**

Performance of the VGOS network in terms of two-dimensional positioning of a lunar lander (upper left) and a corresponding map of VGOS stations (lower right). See *Paper I*.  
*Image credits: Grzegorz Klopotek*

Printed by Chalmers Reproservice  
Chalmers University of Technology  
Gothenburg, Sweden 2017

# Simulation studies of new observing concepts for geodetic Very Long Baseline Interferometry

GRZEGORZ KLOPOTEK

Department of Space, Earth and Environment  
Chalmers University of Technology

## ABSTRACT

Very Long Baseline Interferometry (VLBI) is a space-geodetic technique in which observations are carried out simultaneously by radio telescopes separated by hundreds or thousands of kilometers. The time difference of signal reception between the telescopes is the basic observable used in geodetic VLBI. This technique is capable of determining all five Earth Orientation Parameters (EOP), which provide the connection between the Earth-fixed and space-fixed reference frames. Currently, there is an ongoing effort concerning the establishment of the VLBI Global Observing System (VGOS), which will significantly improve the present measurement precision and increase the total number of observations per session. This requires the key components of the infrastructure, data handling as well as observation approaches to be upgraded and refined. Thus, the focus of this thesis is set on new observing concepts for VGOS. This includes extensive simulations regarding an improved determination of the rotation of the Earth (UT1-UTC) from one-hour VLBI sessions and investigations on the potential of lunar observations in regular geodetic VLBI sessions. The studies summarized in this work address the main topic from two different aspects, providing valuable insights concerning observations in the VGOS era and stimulating new concepts for space geodesy.

**Keywords:** space geodesy, Very Long Baseline Interferometry, VGOS, UT1-UTC, Moon, Monte Carlo simulations, c5++



## RESEARCH CONTRIBUTIONS

This thesis is based on the work comprised of the following contributions:

- I Klotek, G., Hobiger, T., Haas, R., 2017. Geodetic VLBI with an artificial radio source on the Moon: A simulation study. *Journal of Geodesy*. Under review.
- II Kareinen, N., Klotek, G., Hobiger, T., Haas, R., 2017. Identifying optimal tag-along station locations for improving VLBI Intensive sessions. *Earth, Planets and Space* 69, 1–9.
- III Klotek, G., Hobiger, T., Haas, R., 2017. Implementation of VLBI Near-Field Delay Models in the c5++ Analysis Software, in: Nothnagel A. and Jaron F. (Eds.), *Proceedings of the First International Workshop on VLBI Observations of Near-field Targets, October 5 - 6, 2016*, Schriftenreihe des Inst. f. Geodäsie u. Geoinformation, Vol. 54, ISSN 1864-1113, Bonn. pp. 29–33.
- IV Klotek, G., Artz, T., Bellanger, A., Bourda, G., Gerstl, M., Gordon, D., Haas, R., Halsig, S., Hjelle, G.A., Hobiger, T., Hugentobler, U., Iddink, A., Kirkvik, A.S., Lambert, S., Plank, L., Schmid, R., Shu, F., Titov, O., Tong, F., Wang, G., 2016. Results from the VLBI Analysis Software Comparison Campaign 2015, in: Behrend, D., Baver, K.D., Armstrong, K.L. (Eds.), *IVS 2016 General Meeting Proceedings*, International VLBI Service for Geodesy and Astrometry. pp. 203–207.



## ACKNOWLEDGMENTS

I would like to thank everybody at the Department of Space, Earth and Environment for the helpful attitude and assistance during my studies at the Chalmers University of Technology. A very special thanks goes to my co-supervisor Rüdiger Haas for the priceless feedback and for sharing with me his immense experience and knowledge concerning geodetic VLBI. Finally, I would like to express my sincere gratitude to my supervisor Thomas Hobiger for the continuous support, patience and guidance throughout 2.5 years of our cooperation. Without his insightful comments, I would have not been able to bring this thesis to a successful completion.

*Grzegorz*



# CONTENTS

<b>1</b>	<b>INTRODUCTION</b>	<b>1</b>
1.1	Thesis structure . . . . .	2
<b>2</b>	<b>SPACE GEODESY</b>	<b>3</b>
2.1	Celestial & terrestrial reference systems . . . . .	3
2.1.1	Earth Orientation Parameters . . . . .	4
2.2	The Global Geodetic Observing System . . . . .	8
2.2.1	The VLBI Global Observing System . . . . .	9
<b>3</b>	<b>VERY LONG BASELINE INTERFEROMETRY</b>	<b>11</b>
3.1	Principle of geodetic VLBI . . . . .	11
3.2	VLBI delay modelling . . . . .	12
3.2.1	Consensus model . . . . .	12
3.2.2	VLBI near-field delay . . . . .	14
3.2.3	Atmospheric propagation delays . . . . .	16
3.2.4	Displacements of reference points . . . . .	17
3.2.5	Models for technique-specific effects . . . . .	21
3.2.6	Radio source structure . . . . .	21
3.3	Scheduling . . . . .	21
3.4	Observation . . . . .	23
3.5	Processing . . . . .	24
3.6	Analysis . . . . .	26
3.6.1	VLBI database formats for geodetic VLBI . . . . .	26
3.6.2	Ambiguity resolution in bandwidth synthesis . . . . .	27
3.6.3	Parameter estimation . . . . .	27
<b>4</b>	<b>GEODETIC VLBI SIMULATIONS</b>	<b>31</b>
4.1	Tropospheric turbulence . . . . .	32
4.2	Station clock instability . . . . .	34
4.3	Baseline noise . . . . .	34

<b>5</b>	<b>LUNAR OBSERVATIONS WITH GEODETIC VLBI</b>	<b>37</b>
5.1	Geodetic VLBI narrowband observations . . . . .	38
5.1.1	Precision of lunar geodetic VLBI observables . . . . .	38
5.2	BCRS position of an object on the Moon . . . . .	39
<b>6</b>	<b>SUMMARY AND OUTLOOK</b>	<b>41</b>
6.1	Summary of Paper I . . . . .	42
6.2	Summary of Paper II . . . . .	42
6.3	Summary of Paper III . . . . .	43
6.4	Summary of Paper IV . . . . .	43
	<b>BIBLIOGRAPHY</b>	<b>45</b>
	<b>PAPER I</b>	<b>57</b>
	<b>PAPER II</b>	<b>71</b>
	<b>PAPER III</b>	<b>81</b>
	<b>PAPER IV</b>	<b>87</b>

## INTRODUCTION

Technological development, progress in space sciences and advances in signal processing technology allowed geodesy to develop tools which can be used to observe the Earth on global scales. This includes determination of the geometry, the gravity field and the rotation of the Earth as well as the evolution of these parameters in time. Scientists around the globe utilize geodetic data in order to study plate tectonics, fluid dynamics, mass distribution or climate change. Space geodesy does not only facilitate the fundamental understanding of the Earth system but also ensures the continuous availability and timely updates of accurate and stable global reference frames.

The space-geodetic technique used in this thesis is geodetic Very Long Baseline Interferometry (VLBI), which embodies numerous achievements of radio astronomy from the past sixty years. It encompasses also technologies from many fields of science and engineering and combines them into one functional system. The most evident application of geodetic VLBI is the capability to determine all five Earth Orientation Parameters (EOP), which provide the transformation between the Earth-fixed and space-fixed reference frames. Primarily, radio interferometry was developed as a technique used by astronomers to create images of distant celestial objects. Specialized system configurations and dedicated processing chains however enabled also to extract information required for geodetic applications. The improved antenna design, high-speed data recorders and signal calibration systems are just a few examples of equipment which have undergone a significant improvement in geodetic VLBI. The current development of the infrastructure, observing concepts and data handling aims to meet the requirements of the next-generation geodetic VLBI system, namely the VLBI Global Observing System (VGOS) (Petrachenko et al., 2009). The anticipated enhanced measurement precision and continuous geodetic observations will provide scientists with the possibility to determine Earth-based parameters with an unprecedented quality, model subtle global-scale or

local-scale phenomena of various kinds as well as extend the field of space-geodetic research with new applications. The subject of this thesis concerns studies of new observing concepts in the VGOS era and focuses on two aspects, i.e. simulations regarding an improved determination of the rotation of the Earth from one-hour VLBI sessions and investigations on the potential of lunar observations in regular geodetic VLBI sessions. The latter includes the prediction of the performance of this concept through simulations as well as the development of a suitable processing chain for data correlation.

## **1.1 Thesis structure**

The information in this thesis provides a concise overview of geodetic VLBI. Since new observing concepts for VGOS are also presented here, some of the subsections extend the thesis with additional information. First a brief introduction to the terrestrial and celestial reference systems is given in Chapter 2, along with the idea of the Global Geodetic Observing System. In Chapter 3 the main aspects of geodetic VLBI are described including delay modelling, scheduling, observation, correlation and data analysis. Chapter 4 contains information on the modelling of major error sources used in geodetic VLBI simulations. Chapter 5 is related to observations of artificial radio sources by the means of VLBI. This includes the motivation, the current status of geodetic narrowband VLBI and theoretical considerations concerning the precision of lunar observations. Conclusions, an outlook and a brief summary of the attached papers form the final chapter of this thesis.

# Chapter 2

## SPACE GEODESY

The role of space geodesy is fundamental for the understanding of the Earth's dynamics and crucial for quantifying the global changes occurring in the Earth system. Combination of space-geodetic techniques does not only reveal geophysical phenomena in space and time, but also provides accurate and stable reference frames, to which the changes and their variability can be properly referenced.

### 2.1 Celestial & terrestrial reference systems

The International Astronomical Union (IAU) defined two coordinate frames (and 4-dimensional transformation between them), one with its origin in the Solar System Barycenter and one referred to the center of the Earth. These two systems are the Barycentric Reference System (BCRS) with the Barycentric Coordinate Time (TCB) and Geocentric Celestial Reference System (GCRS) with the Geocentric Coordinate Time (TCG) (Petit and Luzum, 2010). The movement of the bodies outside the Earth system is usually expressed in the BCRS and the 'local' GCRS is used for measurements carried out within the Earth system. In both cases, the final orientation of the axes is undefined. It is assumed that their axes are oriented in accordance to those of the International Celestial Reference System (ICRS). The latter is an idealized coordinate system with the origin at the barycenter of the Solar System and non-rotating w.r.t. distant celestial objects. The ICRS is aligned to the mean Earth equator and dynamical equinox of J2000.0 (12<sup>h</sup> Terrestrial Time on 1 January 2000) in order to stay in agreement with previous fundamental reference systems. The first realization of the ICRS at radio frequencies (ICRF1) was adopted by the IAU in 1997. It was based on the positions of stable and point-like extragalactic radio sources with precise coordinates (right ascension  $\alpha$ , declination  $\delta$ ) obtained from a large

number of VLBI observations at S/X bands (Ma et al., 1998). Twelve years later, the ICRF1 was replaced by the second realization of the ICRF (ICRF2), which is used nowadays. The ICRF2 is derived based on a catalog of 3414 (295 defining) compact radio sources from nearly 30 years of VLBI observations. Compared to its predecessor, the ICRF2 is characterized by a more uniform distribution of radio sources and an improved axes stability of about  $10 \mu\text{as}$  (Fey et al., 2009). Currently, ongoing efforts for the realization of the next generation of a VLBI-based International Celestial Reference Frame (ICRF3) are made in order to improve the celestial frame, especially in the southern hemisphere. This implies more sources and better position accuracy and includes also an extension of the ICRF to higher frequencies (Ka,K and Q bands) for practical and scientific applications (Malkin et al., 2015).

There is also a necessity in defining a system similar to the GCRS, but co-rotating with the Earth in its diurnal motion in space. In its resolution from 1991, the International Union of Geodesy and Geophysics (IUGG) defined the International Terrestrial Reference System (ITRS) as a spatial reference system fulfilling the aforementioned requirements. The International Terrestrial Reference Frame (ITRF) realizes this concept using a set of physical points on the Earth with precise positions and velocities. The ITRF is based on the long-term input from four space-geodetic techniques: Global Navigation Satellite Systems (GNSS), Satellite Laser Ranging (SLR), geodetic Very Long Baseline Interferometry (VLBI) and Doppler Orbitography and Radiopositioning Integrated by Satellite (DORIS). The ITRF determination is also complemented by local surveys at co-location sites in order to tie together the reference points of geodetic instruments from different techniques. Due to continuously improved tracking networks and an increasing amount of observations, new realizations of the ITRS were released with the most recent one accessible under the name of ITRF 2014 (Altamimi et al., 2016).

### 2.1.1 Earth Orientation Parameters

Earth Orientation Parameters (EOP) relate the ITRS to the GCRS through a set of rotations. At any given epoch  $t$ , this relation can be expressed as (Petit and Luzum, 2010)

$$\vec{\mathbf{X}}_{GCRS} = \underbrace{Q(t)}_{\text{precession and nutation}} \underbrace{R(t)}_{\text{Earth rotation}} \underbrace{W(t)}_{\text{polar motion}} \vec{\mathbf{X}}_{ITRS}, \quad (2.1)$$

where  $Q(t)$ ,  $R(t)$  and  $W(t)$  refer to transformation matrices (system rotation matrices), which describe motions of the Celestial Intermediate Pole (CIP) in the GCRS, rotation of the Earth around the axis of the CIP and polar motion (motion of the CIP in the ITRS), respectively. EOPs are published by the International

Earth Rotation and Reference Systems Service (IERS) and are available through a dedicated ftp and web service<sup>1</sup>.

The rotations in Eq. 2.1 define a transformation based on the non-rotating origin (NRO), referred to as the Celestial Intermediate Origin (CIO) (Fig. 2.1). Such a reference point allows to decouple the Earth Rotation Angle (ERA) variations from effects due to precession-nutation and polar motion. When referred to the ITRS, the NRO is called the Terrestrial Intermediate Origin (TIO). Conventionally, the initial position of the CIO (of J2000.0) on the equator of the CIP is close to the true equinox of J2000.0 (i.e. the GCRS right ascension origin) and almost stationary in longitude. The motion of the CIO on the celestial sphere over the next few centuries can be approximated by a straight line oriented southwards along the GCRS zero longitude great circle. The plane defined by the geocenter, the CIP and TIO is called *TIO meridian*. The latter is close to the Greenwich meridian (Petit and Luzum, 2010).

### Precession-Nutation

The overall response of the spinning, elastic and oblate Earth to the gravitational attraction of the Moon, Sun and planets causes a movement of the CIP in the celestial reference system. Conventionally, it is described as a smooth long-term motion of about 26,000 years (precession), upon which small periodic components of 18.6 years (nutations) are superimposed. This phenomenon is included in the IAU2006/2000A precession-nutation model (Mathews et al., 2002; Capitaine et al., 2003), from which the celestial pole coordinates  $X$  and  $Y$  can be computed. With them as an input, the  $Q(t)$  matrix can be defined in the CIO-based system transformation (Petit and Luzum, 2010). This includes

$$Q(t) = \begin{bmatrix} 1 - aX^2 & -aXY & X \\ -aXY & 1 - aY^2 & Y \\ -X & -Y & 1 - a(X^2 + Y^2) \end{bmatrix} \cdot R_3(s) \quad (2.2)$$

$$s(t) = -\frac{1}{2} [X(t)Y(t) - X(t_0)Y(t_0)] + \int_{t_0}^t \dot{X}(t)Y(t)dt - (\sigma_0 N_0 - \Sigma_0 N_0), \quad (2.3)$$

with  $a = 1/2 + 1/8(X^2 + Y^2)$  and  $R_3$  as the system rotation matrix around the CIP. The CIO locator  $s$  provides the position of the CIO on the equator of the CIP. The positions of the CIO at J2000.0 and the x-origin of the GCRS are described by  $\sigma_0$  and  $\Sigma_0$ , respectively.  $N_0$  is the ascending node of the CIP equator at J2000.0 in the equator of the GCRS.

The observed differences (in the GCRS) from the modelled motion of the CIP are called celestial pole offsets and are mostly caused by the fact that the free core nutation (FCN), appearing as an additional motion of the CIP, is not a

<sup>1</sup>[www.iers.org/IERS](http://www.iers.org/IERS)

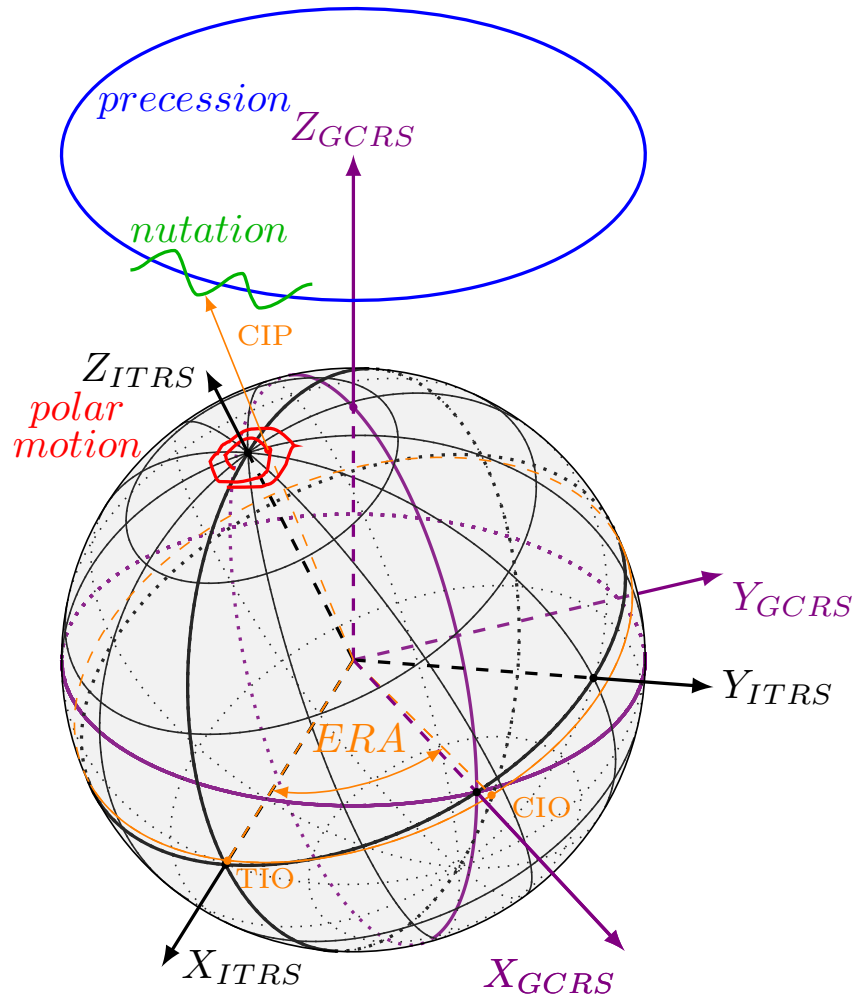


Fig. 2.1: Orientation of the ITRS w.r.t the GCRS in the CIO-based transformation at the date of interest. The description of the used abbreviations can be found in the corresponding subsections.

part of the IAU2006/2000A precession-nutation model. However, the modelled pole coordinates can be refined using celestial pole offsets ( $dX$ ,  $dY$ ) provided by the IERS (Petit and Luzum, 2010).

### Polar motion

Polar motion ( $x_p$ ,  $y_p$ ) describes the movement of the CIP in the ITRS w.r.t the mean rotation pole, i.e. the Earth's axis position in the ICRS at a particular epoch. Besides of the subdaily and daily variations, changes in the  $x_p$  (mea-

sured along the  $0^\circ$  meridian) and  $y_p$  (measured along the  $90^\circ$  W meridian) arise from the annual component and the Chandlerian free motion with a period of approximately 435 days. Smaller variations are almost random and thus polar motion has to be obtained from observations. On the Earth's crust, amplitudes of the CIP motion amount to several meters (Fig. 2.2).

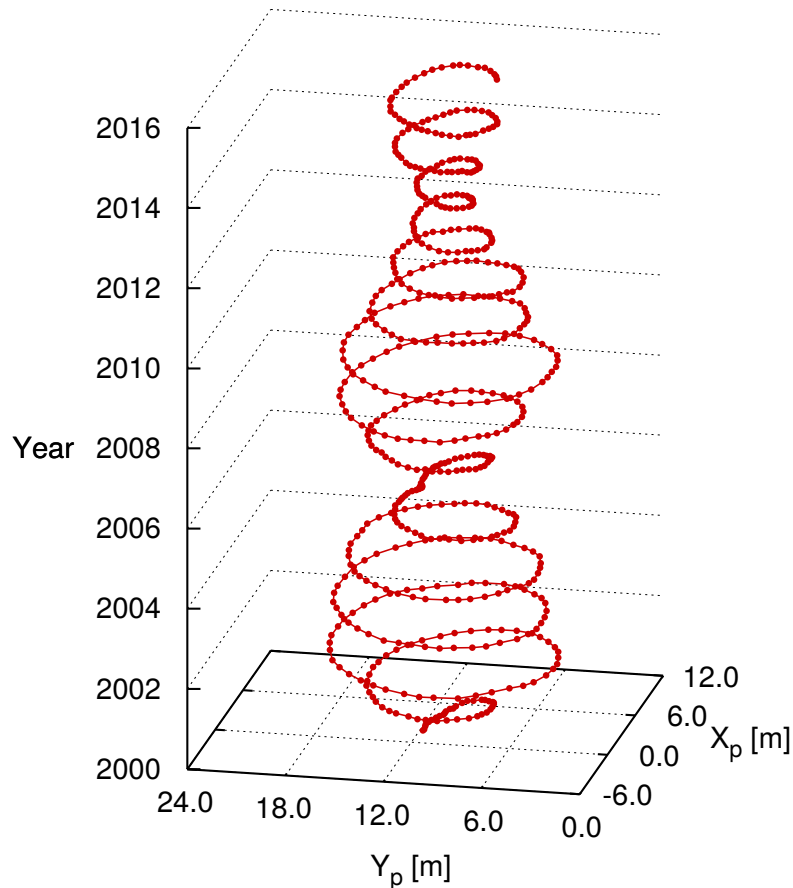


Fig. 2.2: The EOP(IERS) C04 series of polar motion (in meters) shown for the period between the year 2000 and the end of the year 2015 (10 day interval).

The transformation matrix  $W(t)$ , referring to the polar motion at an epoch  $t$ , can be expressed as (Petit and Luzum, 2010)

$$W(t) = R_3(-s') \cdot R_2(x_p) \cdot R_1(y_p) \quad (2.4)$$

$$s'(t) = \frac{1}{2} \int_{t_0}^t (x_p \dot{y}_p - \dot{x}_p y_p) dt, \quad (2.5)$$

with  $t_0$  as the J2000.0 epoch and  $s'$  being the TIO locator, which provides the position of the TIO on the equator of the CIP.

### Earth rotation

The sidereal rotation of the Earth is not uniform and it continuously decreases over time<sup>2</sup>. Usually, it is expressed as the difference between the duration of a day and 86,400 SI seconds (length of the day) or w.r.t the Coordinated Universal Time (UTC). The latter is referred to as the UT1-UTC difference and is defined to be not larger than 0.9 s. In case this threshold is exceeded, an additional second (leap second) is added to the value of UTC.

The rotation of the Earth is expressed conventionally with the Earth Rotation Angle (ERA), which is defined positively in the retrograde direction along the equator of the CIP and between the CIO and TIO. At an epoch  $t$ , the matrix  $R(t)$ , arising from the rotation of the Earth, is then computed as (Capitaine et al., 2000)

$$R(t) = R_3(-ERA) \quad (2.6)$$

$$ERA(T_u) = 2\pi(0.7790572732640 + 1.00273781191135448T_u), \quad (2.7)$$

where  $UT1 = UTC + (UT1-UTC)$  and  $T_u = (\text{Julian UT1 date} - 2451545.0)$ . UT1 is related to the Greenwich mean sidereal time (GMST) and describes the direction of the ITRS zero meridian in the GCRS.

### High-frequency EOP variations

Gravitational forces (mostly luni-solar) of external bodies cause daily and sub-daily variations of the Earth rotation and polar motion. However, these effects are not considered in the EOP series distributed by the IERS. Conventionally, the corresponding corrections  $((\Delta x, \Delta y)_{\text{ocean tides}}, (\Delta x, \Delta y)_{\text{libration}}, \Delta UT1_{\text{ocean tides}}, \Delta UT1_{\text{libration}})$  are computed from models, after interpolation of EOPs to the epoch of interest. The necessity of compensating for such high-frequency effects on a timely basis arises from the fact that their contribution is larger than the current uncertainty of the UT1-UTC and polar motion determination (Chao et al., 1991; Petit and Luzum, 2010; Nothnagel et al., 2016).

## 2.2 The Global Geodetic Observing System

Monitoring of mass redistribution in the global water cycle, climate change and sea level rise are only a few examples of current applications of space geodesy, gravimetry and global geodetic reference frames. In order to better comprehend the phenomena occurring within System Earth, there is a need to augment the current global geodetic infrastructure and improve geodetic and gravimetric measurements in terms of their spatio-temporal coverage and resolution,

---

<sup>2</sup>due to tidal friction. As a consequence, the Moon is spinning away from the Earth at the rate of a few centimeters per year.

latency and quality. The Global Geodetic Observing System (GGOS) aims to address these issues by combining independent observations of the Earth into one consistent frame with the highest possible global accuracy in order to better understand changes of the Earth's shape, rotation, and mass distribution and provide the foundation upon which advances in scientifically and societally vital applications can be made. The GGOS concept was proposed in the early 2000s and became an official component of the International Association of Geodesy (IAG) in 2007. GGOS is based on a wide range of participating organizations, services, institutions and space agencies. With its unique and crucial goals, GGOS is considered to be the 'flagship' project of the IAG<sup>3</sup>.

The establishment of the GGOS requires efforts of many involved parties in various fields. The combination of space geodetic techniques needs upgraded definitions of the terrestrial reference system and its consequent realization based on well-defined standards and conventions. Nowadays, there are numerous independent technique-specific ground-tracking networks providing scientific communities with results of their observations. GGOS will need to coordinate these networks in a sufficient manner in order to assure the consistency within and across the 'three pillars of geodesy' (geometry and kinematics, Earth rotation, and gravity). Moreover, the GGOS concept requires the geodetic community to cooperate with scientists from other fields in order to look at the Earth as one system (Plag and Pearlman, 2009).

### 2.2.1 The VLBI Global Observing System

In the early 2000s, the International VLBI Service for Geodesy and Astrometry (IVS) (Nothnagel et al., 2016) recognized the need to establish the next-generation VLBI system in order to meet the increasing demands on the VLBI technique and be capable to contribute to GGOS. Since then there has been an ongoing effort in upgrading the existing legacy equipment, using additional and broader frequency bands, increasing the number of VLBI stations and improving their global distribution, modifying scheduling approaches or testing new estimation methods in order to enhance the measurement precision to a level of a few picoseconds. This is expected to be achievable in the era of the VLBI Global Observing System (VGOS) (Niell et al., 2005; Petrachenko et al., 2009; Cappallo, 2014; Niell et al., 2014), for which, besides an unprecedented quality of delay observables, a significant increase in the total number of observations per session is expected. The VGOS concept foresees a turnaround time to initial geodetic results of less than 24 hours along with the transition to the continuous monitoring of EOPs and station positions. This should allow to determine the latter with a global accuracy of 1 mm. It is anticipated that VGOS-type measurements will contribute significantly to the quality of prod-

---

<sup>3</sup><http://www.ggos.org/>

ucts available through the IVS and thus provide scientists with a better tool for Earth studies and significantly contribute to the maintenance of terrestrial and celestial reference frames.

# VERY LONG BASELINE INTERFEROMETRY

Very Long Baseline Interferometry (VLBI) is a technique used in radio astronomy where observations are carried out simultaneously by different radio telescopes. These simultaneous measurements are then combined in the process of cross-correlation, producing high-resolution imagery. VLBI enables to observe radio sources with an angular resolution of  $\lambda/D$ , where  $\lambda$  and  $D$  are the observed wavelength and (synthesized) antenna aperture, respectively. The enhanced angular resolution is achieved by increasing the distance between telescopes, which are usually separated by hundreds or thousands of kilometers. Interferometry over long distances can be achieved when radio signals are digitized, time tagged and recorded locally. In astronomy, VLBI provides the highest imaging angular resolution, which allows to observe the emission of very distant natural radio sources in the Universe and, based on this, study the physics behind them. In astrometry, VLBI finds its application in determining the distance and movement of celestial bodies. In geodesy, the observed time delay and its time derivative (delay rate) between two stations forming a baseline can be used for geodynamical studies, EOP determination and maintenance of celestial and terrestrial reference frames.

## 3.1 Principle of geodetic VLBI

Since radio observations are carried out on the surface of the rotating Earth, VLBI delays vary with time. Delay and delay rates depend mostly on the Earth's orientation in the ICRF, radio source positions and the location of VLBI stations. By observing many sources over a longer timespan and at different parts of the world, one can study the orientation and motion of the Earth and

properties of our environment. VLBI observables are useful in examination of geodynamical phenomena happening on the Earth's surface or within its mantle (Ma et al., 1990; Haas and Schuh, 1996). They can also be used for studies of the atmosphere (Behrend et al., 2000). Geodetic VLBI contributes to the maintenance of the ITRF (Bachmann et al., 2016) and it is a unique technique used in realization of the ICRS. It is also the only space-geodetic technique that allows to simultaneously determine all of the Earth Orientation Parameters (Sovers et al., 1998). Data acquisition and dissemination is coordinated by the IVS, which provides highly accurate reference radio source positions, coordinates of radio telescopes and EOPs on a daily basis.

## 3.2 VLBI delay modelling

In order to estimate parameters of interest, the observed delays need to be reduced by their theoretical values for subsequent parameter estimation. In the following section, models used for the computation of the theoretical VLBI delay and approaches for the mitigation of the main error sources are briefly described.

### 3.2.1 Consensus model

Spherical wave fronts, emitted by a very distant natural radio source, become planary by the time they reach the Earth (Fig. 3.1). The time difference of signal reception between two Earth stations forming a baseline can then be expressed in a simple form as

$$\tau_{12}(t) = -\frac{1}{c} \cdot \vec{\mathbf{b}} \cdot \vec{\mathbf{k}}, \quad (3.1)$$

with  $c$  as the speed of light. Here, the direction to the radio source  $\vec{\mathbf{k}}$  and the baseline vector  $\vec{\mathbf{b}}$  are defined in the GCRS. The negative sign is used to express  $\tau_{12}$  as a positive value at the station at which the signal arrives later (remote station). It is assumed that all scalar and vector quantities are computed at the time of arrival at the reference station. The geometric delay  $\tau_{12}(t)$  is a function of time since it changes as the Earth rotates.

In the barycentric frame, the vacuum delay includes also a relativistic term  $\Delta T_{grav}$

$$T_2 - T_1 = -\frac{1}{c} \cdot \vec{\mathbf{K}} \cdot \left( \vec{\mathbf{X}}_2(T_2) - \vec{\mathbf{X}}_1(T_1) \right) + \Delta T_{grav}, \quad (3.2)$$

where  $\vec{\mathbf{K}}$  expresses the unit vector from the barycenter to the source in the absence of gravitational or aberrational bending and  $\vec{\mathbf{X}}_i(T_j)$  is the barycentric position of the  $i^{th}$  station at time  $T_j$ .  $T_2 - T_1$  can be related to the geocentric vacuum

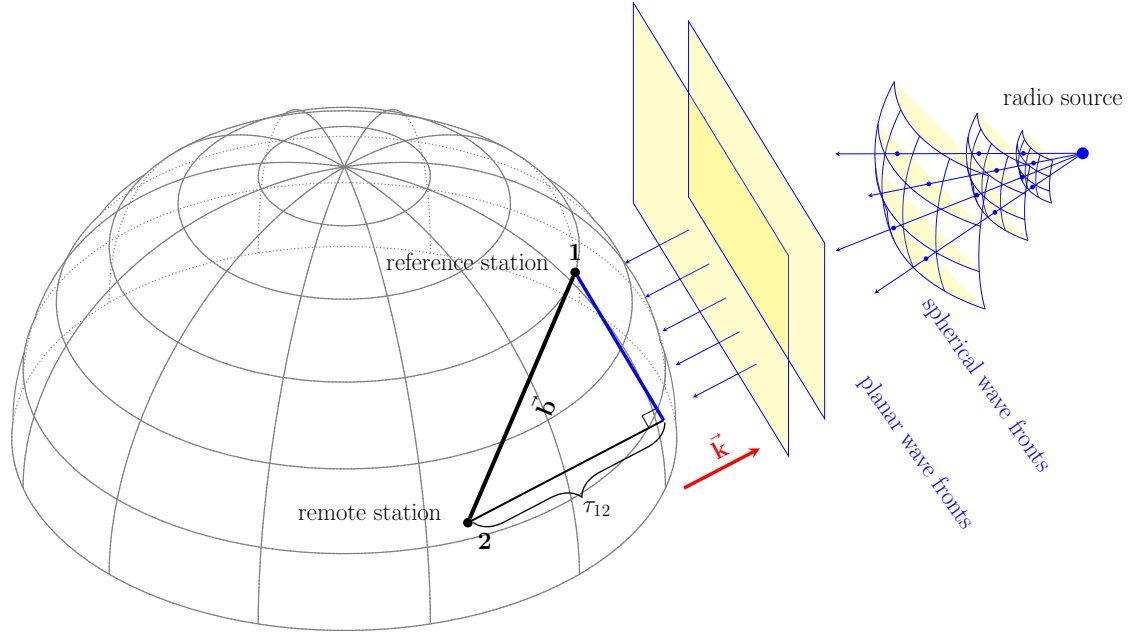


Fig. 3.1: Geometric VLBI delay based on observations to natural radio sources.

delay  $t_{v2} - t_{v1}$  by (Petit and Luzum, 2010)

$$t_{v2} - t_{v1} = \frac{\Delta T_{grav} - \frac{\vec{K} \cdot \vec{b}}{c} \left[ 1 - \frac{(1 + \gamma) U}{c^2} - \frac{|\vec{V}_{\oplus}|^2}{2c^2} - \frac{\vec{V}_{\oplus} \cdot \vec{\omega}_2}{c^2} \right] - \frac{\vec{V}_{\oplus} \cdot \vec{b}}{c^2} \left( 1 + \vec{K} \cdot \frac{\vec{V}_{\oplus}}{2c} \right)}{1 + \frac{\vec{K} \cdot (\vec{V}_{\oplus} + \vec{\omega}_2)}{c}} \quad (3.3)$$

The terms in Eq. 3.3 do not include a change in the geometric delay attributed to the atmospheric propagation delay. If one considers this effect, the time delay reads as

$$t_2 - t_1 = t_{v2} - t_{v1} + \delta t_{atm1} \frac{\vec{K} \cdot (\vec{\omega}_2 - \vec{\omega}_1)}{c}, \quad (3.4)$$

where  $\delta t_{atm1}$  refers to the atmospheric propagation delay at the reference station. The total delay is then found by including other contributions which are briefly described in the following.

In the Solar System the incoming waves are affected by the gravity fields of the Sun and planets. This leads to a change of the time delay and the direction of the signal. Thus, VLBI delays contain also relativistic effects due to space-time curvature

$$\Delta T_{grav} = \sum_J \Delta T_{grav,J}. \quad (3.5)$$

The general relativistic delay  $\Delta T_{grav,J}$  for the  $J^{th}$  gravitating body can be expressed as (Petit and Luzum, 2010)

$$\Delta T_{grav,J} = 2 \frac{GM_J}{c^3} \ln \frac{|\vec{\mathbf{R}}_{1,J}| + \vec{\mathbf{K}} \cdot \vec{\mathbf{R}}_{1,J}}{|\vec{\mathbf{R}}_{2,J}| + \vec{\mathbf{K}} \cdot \vec{\mathbf{R}}_{2,J}} \quad (3.6)$$

$$\vec{\mathbf{R}}_{1,J}(t_1) = \vec{\mathbf{X}}_1(t_1) - \vec{\mathbf{X}}_J(t_{1,J}) \quad (3.7)$$

$$\vec{\mathbf{R}}_{2,J}(t_1) = \vec{\mathbf{X}}_2(t_1) - \vec{\mathbf{X}}_J(t_{1,J}) - \frac{\vec{\mathbf{V}}_{\oplus}}{c} (\vec{\mathbf{K}} \cdot \vec{\mathbf{b}}) \quad (3.8)$$

$$\vec{\mathbf{X}}_i(t_1) = \vec{\mathbf{X}}_{\oplus}(t_1) + \vec{\mathbf{x}}_i(t_1), \quad (3.9)$$

where  $G$  is the gravitational constant,  $M_J$  refers to the rest mass of the  $J^{th}$  gravitating body and  $\vec{\mathbf{R}}_{i,J}$  is the vector from the  $J^{th}$  gravitating body to the receiver at station  $i$ .  $\vec{\mathbf{X}}_{\oplus}(t_1)$  and  $\vec{\mathbf{x}}_i(t_1)$  refer to the barycentric position of the Earth and the GCRS radius vector of the  $i^{th}$  station at time  $t_1$ , respectively.

The gravitational delay in the vicinity of the Earth  $\Delta T_{grav\oplus}$  can be expressed in a simplified form as (Petit and Luzum, 2010)

$$\Delta T_{grav\oplus} = 2 \frac{GM_{\oplus}}{c^3} \ln \frac{|\vec{\mathbf{x}}_1| + \vec{\mathbf{K}} \cdot \vec{\mathbf{x}}_1}{|\vec{\mathbf{x}}_2| + \vec{\mathbf{K}} \cdot \vec{\mathbf{x}}_2}, \quad (3.10)$$

with  $\vec{\mathbf{x}}_i$  defining the GCRS radius vector of the  $i^{th}$  receiver. The total gravitational delay (Eq. 3.5) should include all planets of the Solar System, the Sun and the Moon. When considering observations close to massive bodies or the Sun, the  $\Delta T_{grav}$  term has to be extended with higher order relativistic terms (Klioner, 2003; Petit and Luzum, 2010).

### 3.2.2 VLBI near-field delay

In the case of VLBI and artificial radio sources in the Solar System, the incoming radio waves can not be treated as planary and so-called 'near-field' effects have to be included in the VLBI delay modelling. It is assumed that an object is located in the 'near-field' if the distance  $R$  between the source and an array of telescopes is small compared to  $D^2/\lambda$ , where  $D$  is the synthesized aperture size and  $\lambda$  is the observed wavelength (Born and Wolf, 1970). For X-band observations ( $\lambda \sim 3.5$  cm) and for an aperture size of about 12,000 km, this restricts  $R$  to less than 0.44 light years.

VLBI delay models for radio sources in the 'near-field' and their utilization for observations of spacecrafts are discussed by Moyer (2000), Klioner (2003), Sekido and Fukushima (2006) or by Duev et al. (2012). In the latter study, the time difference of signal reception between two stations is expressed as the difference between two light travel times  $LT_1$  and  $LT_2$  from an artificial object to

the first and second VLBI station. Using the reception time  $T_1$  at the first station, one can determine iteratively the transmission time  $T_0$  of an object

$$T_1 - T_0 = \frac{|\vec{\mathbf{R}}_{01}|}{c} + RLT_{01}, \quad (3.11)$$

with  $|\vec{\mathbf{R}}_{01}|$  referring to the distance between barycentric positions of the first station at the reception time  $T_1$  and the position of the tracked object at its transmission time  $T_0$ . The obtained transmission epoch  $T_0$  is then used to solve for the reception time  $T_2$  at the second observing station using a similar concept as in the case of the  $T_1 - T_0$  difference. (Moyer, 2000; Duev et al., 2012).

The relativistic terms  $RLT_{01}$  or  $RLT_{02}$  should include, similarly to the Consensus model, all planets of our solar system as well as the Sun and the Moon (Moyer, 2000; Duev et al., 2012)

$$RLT_{0A} = \frac{(1 + \gamma) \cdot GM_S}{c^3} \cdot \ln \frac{|\vec{\mathbf{R}}_0^S| + |\vec{\mathbf{R}}_A^S| + |\vec{\mathbf{R}}_{0A}^S| + \frac{(1 + \gamma) \cdot GM_S}{c^2}}{|\vec{\mathbf{R}}_0^S| - |\vec{\mathbf{R}}_A^S| + |\vec{\mathbf{R}}_{0A}^S| + \frac{(1 + \gamma) \cdot GM_S}{c^2}} \quad (3.12)$$

$$+ \sum_{B=1}^{10} \frac{(1 + \gamma) \cdot GM_B}{c^3} \cdot \ln \frac{|\vec{\mathbf{R}}_0^B| + |\vec{\mathbf{R}}_A^B| + |\vec{\mathbf{R}}_{0A}^B|}{|\vec{\mathbf{R}}_0^B| + |\vec{\mathbf{R}}_A^B| - |\vec{\mathbf{R}}_{0A}^B|}, \quad A = \{1, 2\}$$

$$\vec{\mathbf{R}}_i^\alpha = \vec{\mathbf{R}}_i(T_i) - \vec{\mathbf{R}}_\alpha(T_i), \quad i = 0, 1, 2; \alpha = S, B \quad (3.13)$$

$$\vec{\mathbf{R}}_{0A}^\alpha = \vec{\mathbf{R}}_A(T_A) - \vec{\mathbf{R}}_0^\alpha(T_0), \quad \alpha = S, B; A = \{1, 2\}, \quad (3.14)$$

where  $S$  and  $B$  refer to the Sun and a celestial body, respectively. The computation of the  $RLT_{01}$  and  $RLT_{02}$  terms should include the moment of the closest approach of the photon to the gravitating body  $J$  or the position of the gravitating body at the retarded moment of time (Klioner, 2003).

The obtained difference of reception times is expressed in the barycentric dynamical time (TDB) since the motion of the spacecraft and the VLBI telescope reference points are computed in the BCRS (Sekido and Fukushima, 2006). The observed VLBI delays are measured in Terrestrial Time (TT). Therefore, one needs to apply a Lorentz transformation to  $T_2 - T_1$  in order to express the computed geometric delay in the time-scale at the observing stations (Duev et al., 2012)

$$t_2 - t_1 = \left( \frac{T_2 - T_1}{1 - L_C} \cdot \left[ 1 - \frac{1}{c^2} \left( \frac{|\vec{\mathbf{V}}_\oplus|^2}{2} + U_E \right) \right] - \frac{\vec{\mathbf{V}}_\oplus \cdot \vec{\mathbf{b}}}{c^2} \right) \cdot \left( 1 + \frac{\vec{\mathbf{V}}_\oplus \cdot \dot{\vec{\mathbf{r}}}_{2,gc}}{c^2} \right)^{-1}, \quad (3.15)$$

with  $L_C = 1.48082686741 \cdot 10^{-8}$  and  $U_E = \sum_{E \neq j} \frac{GM_J}{r_{Ej}}$  as the Newtonian potential at the geocenter computed for all Solar System bodies excluding the Earth.

$\vec{V}_{\oplus}$  and  $\vec{r}_{2,gc}$  are the barycentric velocity vector of the Earth and the geocentric velocity vector of the second telescope in the GCRS, respectively. The  $t_2 - t_1$  difference is used in the geodetic analysis as the theoretical VLBI delay. The near-field model by Duev et al. (2012) was utilized in simulations concerning lunar observations by the means of geodetic VLBI (*Paper I*) as well as in correlation of the test observations to an artificial radio source on the Moon (*Paper III*).

### 3.2.3 Atmospheric propagation delays

In the last few microseconds of their journey, the incoming radio signals encounter propagation effects while passing through the atmosphere. Although the latter is crucial for any life on the Earth, this medium is rather difficult to handle for scientists dealing with radio observations since it delays and refracts the observed signal. In this subsection, models for atmospheric propagation delays and their utilization for geodetic VLBI are briefly described.

#### Ionospheric delay

The upper part of the atmosphere (50–1000 km) consists of layers of ions and electrons, which affect the propagation of radio signals (refraction, delay, polarization, absorption) with a magnitude proportional to the total electron content (TEC). The latter varies with the local time and depends on the Sun's activity (solar cycle).

Ionospheric delays are frequency-dependent. This allows to obtain ionosphere-free observables  $\tau_0$  using at least two frequency bands and by forming a linear combination of the observed delays (Hobiger et al., 2006)

$$\tau_0 = \frac{\tau_1 f_1^2 - \tau_2 f_2^2}{f_1^2 - f_2^2}, \quad (3.16)$$

where  $f_1, f_2$  are the frequencies of used bands and  $\tau_1, \tau_2$  are the corresponding observed delays. Multiple-frequency band observations are necessary in order to compensate for higher-order ionospheric terms. Their impact however can be neglected in the present measurement precision of VLBI systems (Hawarey et al., 2005; Petit and Luzum, 2010).

#### Tropospheric delay

Any radio signal passing through the lower part of the atmosphere, here often summarized under the term 'troposphere', will be refracted, attenuated and delayed. This additional delay contribution depends on the vertical profile of the atmosphere and the elevation angle of the radio source. The tropospheric delay can be separated into 'dry' (hydrostatic) and 'wet' components. The dry part is

caused by the refractivity of gases in the troposphere. It accounts for most of the total delay and it can be modelled accurately using pressure data from in-situ measurements at a station. Expressed in the zenith direction, the hydrostatic delay (ZHD) can be described as (Davis et al., 1985; Petit and Luzum, 2010)

$$ZHD = \frac{[0.0022768 \pm 0.0000005] P_0}{f_s(\phi, H)} \quad (3.17)$$

$$f_s(\phi, H) = 1 - 0.00266 \cos 2\phi - 0.00000028H, \quad (3.18)$$

where  $P_0$  is the total atmospheric pressure in hPa at the antenna reference point and  $H$  and  $\phi$  refer to the station orthometric height in meters and the geodetic latitude, respectively.

The wet component depends on the amount of the water vapor in the atmosphere, thus being a quantity which is more difficult to model. This is addressed within the geodetic analysis, in which Zenith Wet Delays (ZWD) are estimated along with other geodetic parameters. The line-of-sight (slant) tropospheric delay (TD) can thus be expressed as (Petit and Luzum, 2010)

$$TD = m_h(\varepsilon) ZHD + m_w(\varepsilon) ZWD + m_g(\varepsilon) [G_N \cos(a) + G_E \sin(a)], \quad (3.19)$$

where  $G_N$ ,  $G_E$  are the horizontal delay gradient components. The elevation dependency of the various troposphere delay contributions is expressed through the mapping functions  $m_h(\varepsilon)$ ,  $m_w(\varepsilon)$  and  $m_g(\varepsilon)$  (MacMillan, 1995; Niell, 1996; Böhm et al., 2006).

Usually, the parametrization of the slant delays by the means of ZHD, ZWD, tropospheric gradients and corresponding mapping functions is used in the VLBI analysis. As an alternative approach, tropospheric delays can also be obtained through the ray-tracing method, in which numerical weather models (NWM) are utilized to reconstruct the true path of the incoming signal for subsequent slant delay determination (Hobiger et al., 2008; Hofmeister and Böhm, 2017).

### 3.2.4 Displacements of reference points

Station positions undergo periodic and secular changes, which are triggered by endogenic and exogenic processes, referred to as 'geodynamical phenomena'. These mechanisms are deduced from various geophysical, geodetic and geological measurements as well as based on theoretical considerations. The following subsection focuses on tidal phenomena, which have their major impact on the displacements of reference points. The gravitational pull of celestial bodies causes tidal variations of the ocean and solid Earth which in turn results in displacements of the latter on the level of tens of centimeters and one order of magnitude smaller effects when ocean loading is considered. Other loading

effects should be also taken into account in the analysis of data obtained from space-geodetic techniques (Petit and Luzum, 2010).

### Tide-generating potential

Modelling tidal displacements starts with the description of a gravitational pull of the Moon and the Sun using a harmonic development of the tide-raising bodies, termed 'astronomical tides'. They describe the temporal part on the basis of fundamental tidal frequencies. In general, six astronomical arguments are required for luni-solar tides (Tab. 3.1). This set can be expanded by additional terms, if one considers also contributions of other planets (one argument for each body). However, the impact of the latter is rather small and thus can be neglected (Agnew, 2007).

Table 3.1: Main astronomical arguments (Agnew, 2007). Longitude corresponds to celestial longitude, measured along the ecliptic.

No.	Symbol	Period (d-day, y-year)	Frequency (cycles/day)	Description
I	$\tau$	1.035050 d	0.9661368	Lunar day
II	$s$	27.3216 d	0.0366011	Moon's longitude (tropical month)
III	$h$	365.2422 d	0.0027379	Sun's longitude (solar year)
IV	$p$	8.847 y	0.0003095	Lunar perigee
V	$N'$	18.613 y	0.0001471	Lunar node
VI	$p_s$	20941 y	0.0000001	Solar perigee

The tidal behavior observed on the Earth can be related to a group of astronomical arguments through multiple integer combinations of those, producing in theory an infinite set of tidal frequencies. However, only a small set of such basic frequencies combinations is required in order to represent detectable effects with sufficient accuracy (Tamura, 1987; Kudryavtsev, 2004).

### Solid Earth Tides

The displacement of the solid part of the Earth, at any given location, can be modelled by the tidal potential and so-called load Love and Shida numbers ( $h$ ,  $l$ ). Due to the anelasticity of the Earth's mantle, rotational effects and the presence of oceans, several corrections need to be applied for precise predictions of the deformation. This includes  $h$  and  $l$  to be characterized for the spherical harmonic degree and order ( $m$ ,  $n$ ), expressing latitude dependencies of Love and Shida numbers in terms of additional parameters or by including corrections to these numbers due to the Free Core Nutation effect (Mathews et al., 1995; Agnew, 2007; Petit and Luzum, 2010).

### Ocean Tidal Loading

Similar to solid Earth tides, ocean tides are also induced by the gravitational pull of the Moon and Sun. Water masses driven by those tides cause periodic loading of the ocean bottom that deforms the solid Earth. At a given station, such effects can be observed as horizontal and vertical displacements. Depending on the location, ocean tidal loading can vary from a few millimeters up to several centimeters in the radial component.

The variability of the ocean can be described with a reasonable accuracy as the sum of 11 tides ( $M_2, S_2, N_2, K_2, K_1, O_1, P_1, Q_1, M_f, M_m, S_{sa}$ ) that represent a discrete set of harmonics with the largest amplitudes in the long-period, diurnal and semidiurnal bands. For a given site, the loading caused by ocean tides can be expressed as the sum of horizontal and vertical components (south, west, radial) of a local displacement vector

$$\Delta s = \sum_{k=1}^{11} A_{S_k} \cos(2\pi f_k(t - t_0) + \Phi_k^0(t_0) - \Phi_{S_k}) \quad (3.20)$$

$$\Delta w = \sum_{k=1}^{11} A_{W_k} \cos(2\pi f_k(t - t_0) + \Phi_k^0(t_0) - \Phi_{W_k}) \quad (3.21)$$

$$\Delta r = \sum_{k=1}^{11} A_{R_k} \cos(2\pi f_k(t - t_0) + \Phi_k^0(t_0) - \Phi_{R_k}), \quad (3.22)$$

with  $f_k$  and  $\Phi_k^0$  describing the frequency of the tidal constituent and the phase of the corresponding astronomical argument, respectively. The location dependent coefficients  $A_S, A_W, A_R, \Phi_S, \Phi_W$  and  $\Phi_R$  (per wave) are determined from ocean models. The prediction of ocean loading relies on an expanded set of constituent tides (a total of 342), where 11 main tides are used for spline interpolation of amplitudes and phases of secondary waves (Petit and Luzum, 2010; Scherneck, 2016).

### Body and Ocean Pole Tide Loading

The variability in the rotation of the Earth causes spatial variations in the gravitational potential  $\Delta V(r, \phi, \lambda)$  resulting in tidal effects similar to those triggered by the attraction of external bodies. Although the deformation of the solid Earth caused by the pole tide<sup>1</sup> is small, it cannot be neglected (Petit and Luzum, 2010).

Body pole tide loading in the radial ( $S_r$ ) and horizontal ( $S_\theta, S_\lambda$ ) directions is expressed as (Wahr, 1985)

$$S_r = h_2 \frac{\Delta V}{g}; \quad S_\theta = \frac{l_2}{g} \partial_\theta \Delta V; \quad S_\lambda = \frac{l_2}{g} \frac{1}{\sin \theta} \partial_\lambda \Delta V, \quad (3.23)$$

<sup>1</sup>an effect of the changes in the direction of the Earth's spin axis relative to a point fixed on the Earth

where  $h_2$  and  $l_2$  are the load Love and Shida numbers. In order to model the perturbations of the gravitational potential, observations of the polar motion  $(x_p, y_p)$  are used (Wahr, 1985), i.e.

$$\Delta V(r, \phi, \lambda) = -\frac{\Omega^2 r^2}{2} \sin 2\theta (m_1 \cos \lambda + m_2 \sin \lambda) \quad (3.24)$$

$$m_1 = x_p - \bar{x}_p(t); \quad m_2 = -(y_p - \bar{y}_p(t)), \quad (3.25)$$

with  $r$  as the geocentric distance to the considered point,  $\Omega$  expressing the mean angular velocity of the rotation of the Earth and  $m_1, m_2$  referring to the time-dependent offsets of the instantaneous rotation pole from the mean. The mean pole coordinates  $\bar{x}_p(t)$  and  $\bar{y}_p(t)$  can be calculated with the IERS (2010) mean pole model (Petit and Luzum, 2010).

The centrifugal effect of the polar motion affects also oceans which in turn causes load deformations reaching up to two millimeters in the radial component. The displacement vector in this case is also a function of the  $m_1$  and  $m_2$  parameters and can be computed using the model developed by Desai (2002).

### Tidal atmospheric pressure loading

Diurnal and semidiurnal surface pressure changes induce motions of the Earth's crust, referred to as S1-S2 atmospheric loading. In general, these effects are small and for the regions affected the most (near the equator), the vertical deformations can reach only up to 1.5 mm. However, according to the IERS Conventions (2010), tidal atmospheric pressure loading should be included in the station displacement model.

The station displacement caused by atmospheric pressure can be computed using the S1 and S2 tidal model by Ray and Ponte (2003), which was derived from the European Centre for Medium Range Weather Forecasts (ECMWF) operational surface pressure fields. At any geographic location, the tidal deformation can be expressed as a sum of the vertical, east and north components for both tides by (Petit and Luzum, 2010)

$$d(u, e, n)_{S1} = A_{d1}(u, e, n) \cdot \cos(\omega_1 T) + B_{d1}(u, e, n) \cdot \sin(\omega_1 T) \quad (3.26)$$

$$d(u, e, n)_{S2} = A_{d2}(u, e, n) \cdot \cos(\omega_2 T) + B_{d2}(u, e, n) \cdot \sin(\omega_2 T), \quad (3.27)$$

with location-dependent atmospheric surface displacement coefficients  $A_{d1}, A_{d2}, B_{d1}, B_{d2}$ . Here,  $T$  refers to UT1 expressed as a fraction of a day. The frequencies of the  $S_1$  and  $S_2$  atmospheric tides ( $\omega_1$  and  $\omega_2$ ) are equal to one cycle and two cycles per day, respectively.

### 3.2.5 Models for technique-specific effects

The modelling of the delays needs to include also contributions related to the structure of VLBI antennas. The following subsection highlights the effects that are considered in the conventional VLBI delay modelling.

#### Delays due to antenna axis offsets

In the current VLBI network, some of the antennas are designed in a way that the primary and secondary axes do not intersect. This results in an axis offset (AO), whose contribution to the VLBI delay needs to be considered in the analysis (Sovers et al., 1998; Nothnagel, 2009). In the case of VGOS-type antennas, delays due to antenna axis offsets will be negligible due to the fact that no or sub-millimeter order AO are expected.

#### Delays due to thermal deformation

Thermal expansion of the mechanical parts of VLBI telescopes causes displacements of VLBI antenna reference points w.r.t. their mean positions. Such an additional delay can be modelled according to Nothnagel (2009), who considered station-dependent parameters (expansion coefficients, dimensions of the telescope, focus factors, reference air temperature) for the empirical delay model.

### 3.2.6 Radio source structure

The ICRF position of the radio source refers to the radio centroid (da Silva Neto et al., 2002) and any variation in the structure is revealed as a small change of the right ascension and declination coordinates. Therefore, a regular monitoring of the sources used in geodesy and astrometry is essential in order to investigate the stationarity of quasars, refine their position or update the group of sources realizing the ICRF.

## 3.3 Scheduling

Geodetic VLBI relies on measurements to many radio sources at different elevation angles and telescopes distributed around the world. Thus, careful scheduling is crucial since it directly affects the quality of the geodetic parameters. Creating an optimal observing schedule is a complex subject and many factors need to be taken into account. The designed schedule should be as efficient as possible and contain a maximum number of observations, which implies minimum slewing and idle times between the measurements. The observed sources need to have a high flux density, be compact (point-like) and should

have well-established coordinates. Observations should be carried out at different azimuth and elevation angles in order to solve for atmospheric parameters. Most importantly, the measurement time should be long enough in order to achieve a proper signal-to-noise ratio (SNR), which in turn affects the precision of a group delay observable (Takahashi et al., 2000).

Determination of the minimum observation times in a scan requires the knowledge about sources flux densities and performance of the receiving systems at each station. The minimum observation time is usually chosen to match a predefined SNR. For natural radio sources and the legacy S/X systems, this value is usually in the range between 15 and 20.

The SNR of an interferometric observation can be expressed as (Shaffer, 2000)

$$\text{SNR} = \frac{\eta_c S_c \sqrt{2 \cdot B_{eff} \cdot T_{int}}}{\sqrt{\text{SEFD}_1 \cdot \text{SEFD}_2}} \quad (3.28)$$

$$\text{SEFD}_i = \frac{2kT_{S_i}}{A_{e_i}}, \quad i = \{1, 2\}, \quad (3.29)$$

where  $B_{eff}$  is the effective bandwidth in Hz and  $T_{int}$  refers to the integration (observation) time. The system equivalent flux density (SEFD) of an observing system relates to the Boltzmann constant  $k$ , the system temperature  $T_S$  and the antenna effective aperture  $A_e$ . The efficiency factor  $\eta_c$  is associated with the losses due to the signal digitization.  $S_c$  is the correlated flux density of an observed source in units of Jansky ( $1 \text{ Jy} = 10^{-26} \text{ Wm}^{-2} \text{ Hz}^{-1}$ ). In the case of near-field objects, even a faint radio transmitter usually has a much higher flux density than any of the natural radio sources considered in geodetic VLBI. This implies that the SNR targets would be reached very fast, thus allowing for scheduling of very short scan times.

Scheduling should be complemented by a performance analysis of the designed VLBI networks in terms of the sensitivity w.r.t. the target parameters. For instance, long east-west baselines are more sensitive for measuring the Earth rotation phase (i.e. UT1-UTC difference). On the contrary, a global distribution of VLBI stations is required in order to determine the polar motion in a reliable manner (Nothnagel and Schnell, 2008; Nothnagel et al., 2016).

Routine VLBI sessions for geodetic and astrometric purposes are organized by the IVS and involve VLBI stations distributed around the globe. The observing schedules are available through so-called VLBI experiment (VEX) files (Whitney et al., 2002), which can be downloaded from one of the IVS servers<sup>2</sup>. The yearly observing programs consist mostly of the daily one-hour VLBI 'Intensive sessions' as well as 24-hour VLBI observations that are carried out twice a week as so-called 'rapid turnaround' sessions (Nothnagel et al., 2016). Global IVS sessions are listed in Tab. 3.2. In addition, a number of other experiments are also

---

<sup>2</sup><ftp://gemini.gsfc.nasa.gov/>

carried out for various purposes including regional network monitoring and scientific studies<sup>3</sup>.

Table 3.2: Global IVS observing programs.

Session Name (Abbreviation)	Frequency	Duration	Purpose
Intensive 1 (IVS-INT1)	Monday – Friday	1 hour	UT1-UTC determination
Intensive 2 (IVS-INT2)	Weekends		
Intensive 3 (IVS-INT3)	Mondays		
Rapid-turnaround 1 (IVS-R1)	Mondays	24 hours	EOP & TRF determination
Rapid-turnaround 4 (IVS-R4)	Thursdays		
Research & development (IVS-R&D)	Several per year	24 hours	Specific scientific and technical goals
CRF (IVS-CRF)	Several per year	24 hours	ICRF improvement and densification
TRF (IVS-T2)	Bi-monthly	24 hours	TRF monitoring
VLBA (IVS-RDV)	Several per year	24 hours	Various geodetic/astrometric applications
Continuous VLBI campaign (CONT)	Every three years	Two weeks	State-of-the-art VLBI data

### 3.4 Observation

After being reflected by an antenna and focused into the feed, the incoming electromagnetic waves are converted to an electrical voltage signal (RF) and amplified by the Low-Noise-Amplifier (LNA). At this stage, the phase calibration tones (phase-cal) are also injected. The phase-cal signal consists of a set of distinct tones separated by a few MHz and is utilized to determine the relative phases between channels (Cappallo, 2014). After amplification, the RF signals are down-converted from the sky frequency (RF) to the intermediate frequency (IF) and enter a digital back-end (DBE). Nowadays, almost all stations are equipped with a DBE such as the Digital Base-Band Converter (DBBC) (Tucari et al., 2006, 2010, 2014). The IF signals are separated there into a predefined

<sup>3</sup><https://ivscc.gsfc.nasa.gov/>

set of narrow channels per frequency band<sup>4</sup>, converted to baseband frequencies, digitized with a certain quantization (sampling) level, time-tagged based on the 1PPS (Pulse-per-second) signal from a hydrogen maser (H-maser), formatted (e.g., Mark 5, Mark 6, VDIF) and transferred to the recorder (in-situ recording systems, direct data streaming to the correlator) (Whitney, 2004; Whitney et al., 2014; Salminen, 2015).

If there are changes in the length of the cable (stretching and twisting due to the antenna motion or temperature changes) which delivers the RF signal from the antenna to the DBE, additional systematic errors will occur. This issue is addressed by utilizing the cable delay measurement system, with which measurements are carried out right before and after each observation. An additional length of a cable is also attached to the signal path before and after each session in order to determine the cable sign (sense). The latter is needed in order to convert the cable calibration data into the corresponding group delay contribution, which is included later in the data analysis.

The acquisition of the VLBI data at each station is controlled and carried out automatically by the Field System (FS) (Himwich, 2000). During the experiment, the FS steers the antenna using commands sent to the telescope control system in accordance to the station schedule. For each scan, the FS writes also a set of parameters into a log-file, which is then used during the data correlation and subsequent geodetic analysis. Such station log-files contain meteorological readings (temperature, pressure, wind speed and direction, relative humidity), cable delay data and measurements of the time difference between the GPS time and the time standard provided by the H-maser.

### 3.5 Processing

The processing part of geodetic VLBI consists of the correlation of raw observations and the geodetic observables extraction based on the correlator output. In the following subsection, correlation and fringe-fitting are briefly described.

#### Correlation

Once the observing session ends, data are transferred to the correlation center for subsequent processing, during which the recorded signals are compared in the process of cross-correlation to determine differences in signal arrival times between stations. For each baseline, recorded signals are shifted in time relative to each other by  $\tau$  until its cross-correlation function is maximized (Sovers et al., 1998). This was realized in the past using XF-style correlators, but nowadays

---

<sup>4</sup>For the data rate of 256 Mbps and the bandwidth of 128 MHz, it is usually 8 channels 8 MHz wide for X-band and 6 channels 8 MHz wide for S-band.

FX-style correlators such as the Distributed FX (DiFX) (Deller et al., 2007) software correlator are used to process the VLBI observations. In the case of a FX-type correlator, the complex visibilities (correlation amplitudes and interferometric phases) are obtained by a Fourier Transform (F) and cross-multiplication (X) of the digitized data streams.

In order to correlate the data from a number of different telescopes, the geocentric VLBI delay must be calculated in regular intervals<sup>5</sup> per telescope to align all the data to a common point (geocenter). Once this is done and phases are corrected after fringe rotation, the data are converted from the time- to frequency-domain, using the Fast Fourier Transform (FFT). Next, the channelized data are cross-multiplied to obtain the complex visibilities for each band, polarization and baseline. Finally, the results are time-averaged for a given accumulation period and saved for subsequent processing.

### Fringe-fitting

The time difference of signal reception between two stations can be expressed as an interferometric phase. In astrometric differential VLBI, most of the phase errors are removed by alternate observations of target sources with nearby calibrators. In the case of geodetic observations, it is hard to obtain phase delay if the theoretical models are imprecise (telescope or source position errors, GPS clock errors, telescope path-length changes) and unmodelled phase errors exist (residual tropospheric and ionospheric short-term variations, instrumental errors). For the baselines on the order of few thousand of kilometers, this implies a problem in solving for the phase delay ambiguities, which need to be known prior to the geodetic analysis (Herring, 1992) (cf. Sec. 3.6.2). Therefore, group delay observables  $\tau_{gd}$  are used in geodetic VLBI instead. They are obtained by measuring the rate of change of the phase with frequency and are determined through the bandwidth synthesis technique (Sovers et al., 1998; Rogers, 1970). In this approach, the bandwidth is virtually increased by utilization of several few MHz wide channels, spread out over a much larger bandwidth. The group delay is then found by estimating the linear phase change across multiple channels by synthesizing all the channels, leading to an enhanced precision of group delay observables. During the 'fringe-fitting', the best estimates of residual delays and delay rates are obtained, where a two-dimensional Fourier transform of the cross-correlation spectra is used to find the peaks of the function in time (group delay) and frequency (delay rate) domains. When added to modelled quantities, they express the absolute values of these parameters (Takahashi et al., 2000). Fringe-fitting provides singleband delays (SBD), multi-band delays (MBD) and delay rates. In theory, the SBD for each IF channel

---

<sup>5</sup>The delays are interpolated to the specific observation time, while including the station clock offsets and rates.

should be the same. Due to instrumental errors however, each IF channel is characterized by its own phase offset and slope. As mentioned in Sec. 3.4, this problem is dealt with by making use of the PCAL signals, which are injected at the receiving stage and during the whole observation period.

The *fourfit* software of the Haystack Observatory Post-processing System (HOPS)<sup>6</sup> is the common fringe-fitting program that is used in connection with correlator centers in order to process quasar observations and provide the scientific community with data for subsequent analysis.

## 3.6 Analysis

VLBI data analysis allows us not only to estimate VLBI station positions and EOPs but also various parameters related to the signal propagation or the Earth's dynamics. This can be done based on individual experiments or during a global analysis, in which observations from many experiments are combined. In the following section, a brief description of various aspects of VLBI data analysis is given.

### 3.6.1 VLBI database formats for geodetic VLBI

Once the post-correlation processing is done, VLBI observables and related information are stored into databases, which are then made available through the IVS<sup>7</sup>. Currently, there are several different database formats used for VLBI data analysis. They differ in terms of their flexibility, data structure and amount of information stored.

The Mark III database (MK3-DB) (Gipson, 2012) is a binary format used to store the correlation output and some auxiliary information such as meteorological data or geophysical models. There are different versions of those databases, where version numbers indicate the degree of modifications made to the data. As an example, version-1 databases consist of the raw correlator output, whereas version-4 databases (final) contain modified observables (ambiguity- and ionosphere-free group delays, removed outliers) and external data (precomputed parameters, cable delay values, meteorological data). Based on the latter version, a subset of data crucial for VLBI analysis is also exported to so-called National Geodetic Survey (NGS) cards<sup>8</sup>. Such data are the starting point for some VLBI analysis packages since human-readable content stored in a single ASCII file allows for an easy-to-implement data interface.

In order to meet the increasing requirements of VGOS (large amounts of data, new observables and stations), the VLBI Global Observing System Data

<sup>6</sup><http://www.haystack.mit.edu/tech/vlbi/hops.html>

<sup>7</sup><ftp://cddis.gsfc.nasa.gov/pub/vlbi/ivsdata/>

<sup>8</sup>[ftp://cddis.gsfc.nasa.gov/pub/reports/formats/ngs\\_card.format](ftp://cddis.gsfc.nasa.gov/pub/reports/formats/ngs_card.format)

Base (vgosDB) became recently the new VLBI data format, replacing the MK3-DB and providing a more compact data structure with an enhanced performance (Gipson, 2014). vgosDB is based on the Network Common Data Form (NetCDF) format<sup>9</sup>, an open standard designed for fast data access and commonly used in the scientific community. Similarly to MK3-DB, the vgosDB format provides all the data associated with the correlation process as well as some external information. Data belonging to a certain scope (scan, observation, station) are archived in separate directories, in which data are stored in individual NetCDF files, depending on their origin and use. In this way, observables are kept separate from a priori values or meteorological data. Access to specific session files is achievable through a so-called 'wrapper', which is an ASCII file located in the main session directory. The vgosDB concept is depicted in Fig. 3.2. Currently, IVS data in the vgosDB format are provided in parallel with MK3-DB and NGS cards, until the full transition to the new format is complete.

### 3.6.2 Ambiguity resolution in bandwidth synthesis

The bandwidth synthesis technique allows to increase the precision of the determined group delays without the necessity of having single-channel bandwidths of a GHz or more. However, the obtained observables contain an unknown number of integer ambiguities. They need to be known prior to the VLBI analysis, because any unresolved ambiguities will propagate to the estimated geodetic parameters. Fortunately, the group delay ambiguity spacing  $\tau_{amb}$  is quite large and is defined as the inverse of the greatest common measure of the frequency spacing (Takahashi et al., 2000). For a typical geodetic VLBI frequency setup (IVS-R1, IVS-R4), it amounts to 50 ns and 100 ns for X- and S-band, respectively. The ambiguity resolution can be carried out in an iterative approach by choosing a number of ambiguities in X/S bands in a way that they minimize the WRMS values from the estimation process, for which a simple parametrization (clock polynomials and local tropospheres) is applied (Hobiger et al., 2010; Kareinen et al., 2016). After each solution (iteration), the ambiguities are shifted in accordance to the obtained residuals. It is assumed that all ambiguities are detected properly if the residuals are much smaller than the aforementioned ambiguity spacings. Once the ambiguities are resolved, the X- and S-band data are utilized in order to compute ionosphere delay corrections, resp. ionosphere-free observables (Eq. 3.16).

### 3.6.3 Parameter estimation

There are many software packages capable of performing VLBI data analysis, which allow to estimate a wide range of geodetic parameters. A list of such

<sup>9</sup><http://www.unidata.ucar.edu/software/netcdf/>

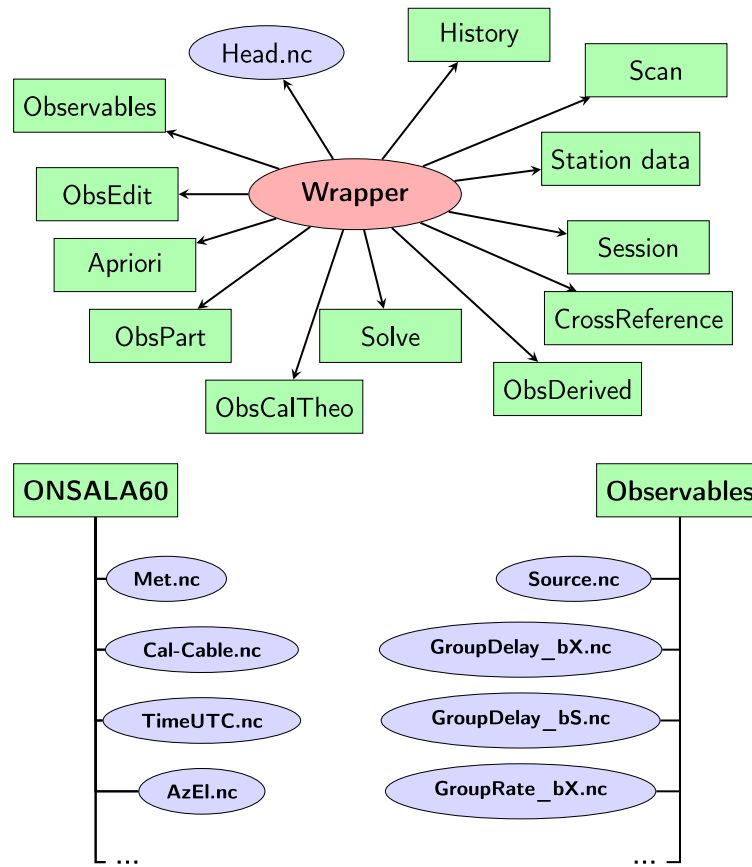


Fig. 3.2: Organization of data in the vgosDB format. The scope-specific \*.nc files (purple ellipses) are stored in different directories (green rectangles). The data access is managed using wrappers (red ellipse), which contain the names of directories and files stored in the created database.

packages includes e.g., *Calc/Solve* (Ma et al., 1990), *OCCAM* (Titov et al., 2004),  *$\nu$ Solve* (Bolotin et al., 2014), *VieVS* (Böhm et al., 2006) or *c5++* (Hobiger et al., 2010). The latter package was used for the geodetic VLBI simulations, summarized in *Paper I* and *Paper II*. *c5++* was also utilized to compute near-field VLBI delays for correlation of lunar observations (*Paper III*). In *Paper IV* the comparison of VLBI analysis softwares on the basis of computed theoretical delays is described. In this subsection the main aspects of data analysis are highlighted.

The quantity and type of estimated parameters depend mostly on the analyzed session. Due to the low number of participating stations and short session duration, there are only a few observations in the VLBI Intensive sessions. In the case of INT1 and INT2, six parameters are commonly estimated i.e. three clock polynomial coefficients w.r.t the reference clock, ZWD for both stations

and the UT1-UTC difference. A more comprehensive analysis can be carried out with 24-hour sessions such as IVS-R1, IVS-R4 or IVS-T2, where one can estimate EOPs (polar motion and UT1-UTC), station coordinates and various additional parameters. If all station coordinates are solved in the VLBI analysis, the singularity of the normal-equation matrix has to be dealt with by introducing No-Net-Translation (NNT) and No-Net-Rotation (NNR) conditions w.r.t. the a priori coordinates. Source coordinates are set to their a priori values, but the parametrization can also include radio source positions if some of them e.g., exhibit a varying structure. EOPs and station positions are derived once per 24 hours, while nuisance parameters are estimated every few hours. The behaviour of frequency standards at VLBI stations and the troposphere is well represented using a piece-wise linear (PWL) parametrization. Station clock differences w.r.t. the chosen reference H-maser are estimated typically with an one-hour interval. The atmospheric delay is estimated according to Eq. 3.19, where ZWD and tropospheric gradients are determined usually every two and six hours, respectively. Care has to be taken however when estimating global, daily or stochastic parameters. There is no universal parametrization optimal for all cases and for all data sets and the analyst has to decide on the number of estimated parameters, used weights or applied constraints.

#### **c5++**

The *c5++* analysis software was developed in cooperation between the National Institute of Information and Communications Technology (NICT), Japan Aerospace Exploration Agency (JAXA), and Hitotsubashi University. The developer group currently includes also Chalmers University of Technology. The software is written in C++ and can be utilized for the processing of VLBI, GNSS and SLR data separately or in a multi-technique mode, in which different types of data are combined on the observational level (Hobiger and Otsubo, 2014). Unlike *νSolve* or *VieVS*, *c5++* does not have a Graphical User Interface (GUI). It has to be controlled through a configuration file, in which analysis options and target parameters are defined. Therefore, it is fully controllable with external scripts and suitable for automatic analysis of VLBI data. *c5++* supports data reading from MK3-DB, vgosDB, NGS cards and the raw correlator output from the K5 system. Recently, this software was extended with a VLBI simulation module, capable of generating synthetic VLBI observables. This is useful for simulation studies concerning new observing concepts for geodetic VLBI.



## GEODETIC VLBI SIMULATIONS

Simulation studies are an effective tool for predicting the performance of new concepts or technology in case no real observations are available. For example, extensive Monte Carlo simulations were carried out during the design phase of the VGOS system in order to investigate the impact of different scheduling strategies, network sizes and error sources on estimated geodetic parameters (Petrachenko et al., 2009). Monte Carlo simulations rely on the idea to characterize the performance of a model through repeated statistical sampling. This requires a mathematical model and some input parameters with known probability distributions. Given the random variation in the input data, a large number of simulations provide then the basis for deriving empirical statistical information. There should be always a large number of independent simulation runs in order to achieve a realistic approximation of the probability distribution of the outcome values (Kareinen et al., 2015).

In the case of geodetic VLBI, group delay observables can be simulated as the sum of the geometric VLBI delay  $\tau_g$  (near-field or far-field) and three major error sources, i.e. water vapor fluctuations (zenith wet delays  $ZWD_1$  and  $ZWD_2$ ), instability of station clocks ( $clk_1$ ,  $clk_2$ ) and thermal noise of the observing systems at stations forming a baseline ( $\tau_{rnd}$ ). This can be expressed as

$$\tau_{sim} = \tau_g + (ZWD_2 \cdot m_w(\varepsilon_2) + clk_2) - (ZWD_1 \cdot m_w(\varepsilon_1) + clk_1) + \tau_{rnd}, \quad (4.1)$$

with  $\varepsilon_j$  as a source elevation angle at the  $j^{th}$  station. Zenith Wet Delay (ZWD) time series can be simulated following the turbulence model (Treuhaft and Lanyi, 1987) described by Nilsson et al. (2007) or by (Halsig et al., 2016). Each simulated  $ZWD$  value is mapped to the source elevation angles using wet mapping functions  $m_w$  (cf. Eq. 3.19). The behavior of the VLBI station clocks  $clk$  is modeled as the sum of random walk and integrated random walk processes (Herring et al., 1990). The thermal noise contribution  $\tau_{rnd}$  is modeled as a Gaussian white noise process. Compared to the formal errors, i.e. the precision of

parameters from the design matrix of a least-squares adjustment, Monte Carlo simulations allow us to study also the accuracy of target parameters since the 'true' values are known. In *Paper I* and *Paper II* this statistical method is used for studies concerning geodetic VLBI observations of an artificial lunar radio source and UT1-UTC determination, respectively.

## 4.1 Tropospheric turbulence

Dynamic processes in the troposphere induce spatial and temporal refractivity variations, which affect the radio wave propagating through the atmosphere. Besides of the variability in the amplitude of the signal, a turbulent medium causes also rapid changes in the atmospheric delay. Fluctuations of water vapor along the propagation path are non-negligible. Such delays are considered as a dominant error source, which affects the determination of geodetic parameters. Simulations of the propagation delays of radio signals can be useful when aiming to improve the overall performance of space-geodetic techniques or validate newly developed concepts (Treuhaft and Lanyi, 1987; Hallsig et al., 2016).

The propagation of radio signals through a turbulent medium can be described by the Kolmogorov turbulence theory. Thereby, it is assumed that the temporal fluctuations over a site are caused by spatial variations driven by the wind (Taylor's frozen flow hypothesis). Correlations between the refractivity index at two locations ( $\mathbf{r}_i, \mathbf{r}_j$ ) or epochs ( $t_i, t_j$ ) can be defined as (Tatarskii, 1971; Treuhaft and Lanyi, 1987)

$$\langle (n_i - n_j)^2 \rangle = C_n^2 \frac{\|\mathbf{r}_i - \mathbf{r}_j + \mathbf{v}\delta t_{ij}\|^{2/3}}{1 + \frac{\|\mathbf{r}_i - \mathbf{r}_j + \mathbf{v}\delta t_{ij}\|^{2/3}}{L^{2/3}}}, \quad (4.2)$$

where  $C_n$  is called the refractive index structure constant ( $\text{m}^{-\frac{1}{3}}$ ),  $\mathbf{v}$  is the wind speed,  $\delta t_{ij} = t_i - t_j$  and  $L$  is the turbulence saturation scale length (m). The elements  $[C_{ij}]$  of the parameter covariance matrix can be computed in accordance to Nilsson et al. (2007) and Nilsson and Haas (2010) as

$$[C_{ij}] = \frac{C_n^2}{2} \int \int \left[ \frac{\|\mathbf{r}_i(z) - \mathbf{r}_0(z') + \mathbf{v}\delta t_{i0}\|^{2/3}}{1 + \frac{\|\mathbf{r}_i(z) - \mathbf{r}_0(z') + \mathbf{v}\delta t_{i0}\|^{2/3}}{L^{2/3}}} + \frac{\|\mathbf{r}_j(z) - \mathbf{r}_0(z') + \mathbf{v}\delta t_{j0}\|^{2/3}}{1 + \frac{\|\mathbf{r}_j(z) - \mathbf{r}_0(z') + \mathbf{v}\delta t_{j0}\|^{2/3}}{L^{2/3}}} \right. \\ \left. - \frac{\|\mathbf{r}_i(z) - \mathbf{r}_j(z') + \mathbf{v}\delta t_{ij}\|^{2/3}}{1 + \frac{\|\mathbf{r}_i(z) - \mathbf{r}_j(z') + \mathbf{v}\delta t_{ij}\|^{2/3}}{L^{2/3}}} - \frac{\|\mathbf{r}_0(z) - \mathbf{r}_0(z')\|^{2/3}}{1 + \frac{\|\mathbf{r}_0(z) - \mathbf{r}_0(z')\|^{2/3}}{L^{2/3}}} \right] dz dz'. \quad (4.3)$$

The double integral in Eq. 4.3 can be replaced by numerical integration. Once the  $C$  matrix is obtained, a vector of simulated ZWD values  $\mathbf{l}^z$  can be generated using

$$\mathbf{l}^z = l_0^z + D\mathbf{x}; \quad C = DD^T, \quad (4.4)$$

with an a priori zenith wet delay  $l_0^z$ ,  $\mathbf{x}$  as a vector of random numbers derived from the standard normal distribution and  $D$  being the lower triangular matrix of the Cholesky factorization from the decomposition of the covariance matrix  $C$ . Finally, the simulated ZWD values can be mapped to the slant directions using  $m_w$  (cf. Eq. 3.19). As an example, simulated ZWDs at four VLBI stations are shown in Fig. 4.1.

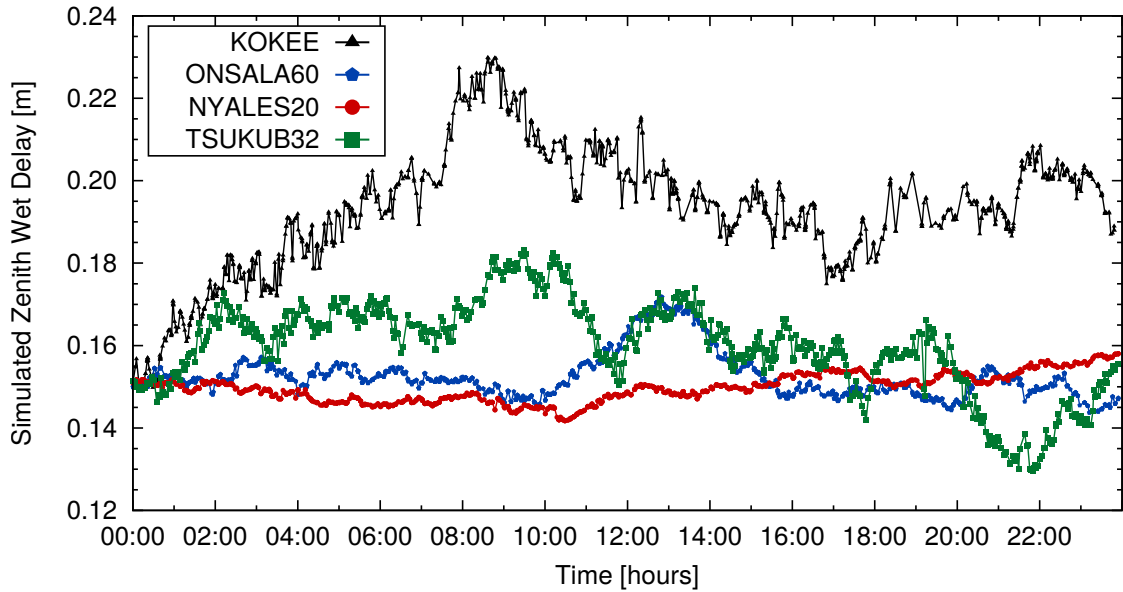


Fig. 4.1: Examples of simulated ZWD time series at four VLBI stations: KOKEE ( $C_n = 2.05 \cdot 10^{-7} \text{ m}^{-\frac{1}{3}}$ ,  $H_{trop} = 2026.2 \text{ m}$ ), ONSALA60 ( $C_n = 0.72 \cdot 10^{-7} \text{ m}^{-\frac{1}{3}}$ ,  $H_{trop} = 1756.6 \text{ m}$ ), NYALES20 ( $C_n = 0.35 \cdot 10^{-7} \text{ m}^{-\frac{1}{3}}$ ,  $H_{trop} = 1844.7 \text{ m}$ ), TSUKUB32 ( $C_n = 1.54 \cdot 10^{-7} \text{ m}^{-\frac{1}{3}}$ ,  $H_{trop} = 1850.4 \text{ m}$ ).  $ZWD_0 = 0.150 \text{ m}$ , wind speed of 7 m/s and  $L = 3000 \text{ km}$  are the basic input parameters for the turbulence model.

Besides of  $l_0^z$  and the wind speed  $\mathbf{v}$ , which can be obtained from the numerical weather prediction models, several other input parameters of the turbulence model need to be defined or determined beforehand in order to simulate time series of ZWD. Following Treuhft and Lanyi (1987), the saturation length scale  $L$  should be between 1400 and 3000 km.  $C_n$  is usually assumed to be constant up to an effective tropospheric height  $H_{trop}$  (thickness of the turbulent layer) and zero above that. Average  $C_n$  and  $H_{trop}$  values per site can be obtained from radar measurements, Water Vapor Radiometers, radiosondes or thermosondes data (Rao et al., 2001; Nilsson et al., 2005; Azouit and Vernin, 2005; Vasseur,

1999). Similar information can also be obtained from GNSS (Nilsson et al., 2009). In the case of geodetic VLBI simulations, the  $C_n$  and  $H_{trop}$  values for different sites are taken from Petrachenko et al. (2009). It should however be noted that a seasonal variability in the magnitude of the  $C_n$  parameter (larger in summer than in winter) exists, which one could take into account when simulating longer periods of time.

## 4.2 Station clock instability

Received, down-converted and digitized signals are time-tagged at VLBI stations using the 1PPS signal from the H-maser. The stochastic behaviour of a frequency standard can be accessed and characterized by the Allan deviation  $\sigma(\tau)_{ADEV}$  (ADEV) or the Overlapping Allan deviation  $\sigma(\tau)_{OADEV}$  (OADEV)<sup>1</sup> (Howe et al., 1981). The Allan deviation as a function of the averaging period  $\tau$  allows to identify the magnitude and type of the noise affecting the clock signal. In the case of real VLBI clocks, the computed Allan deviation decreases steady for  $\tau$  up to about an hour. For larger averaging intervals,  $\sigma(\tau)_{ADEV}$  tends to increase. On a logarithmic scale, this corresponds to two slopes of  $-1/2$  and  $1/2$ . Therefore, the clock behavior can be simulated as the sum of random walk and integrated random walk processes (Herring et al., 1990; Wresnik, 2009). As an example, the stability characteristics computed for the simulated behavior of four VLBI station clocks is shown in Fig. 4.1 using OADEV.

## 4.3 Baseline noise

The baseline noise  $\tau_{rnd}$  in Eq. 4.1 corresponds to the performance of the measurement systems at VLBI sites and can be attributed to the thermal noise of the receiving chains. For the simulations of present geodetic VLBI quasar observations,  $\sigma$  of the Gaussian distribution can be set to 40–60 ps. This corresponds to a thermal noise of 12–18 mm and reflects the average post-fit RMS of today’s geodetic VLBI. In the case of VGOS-type observations,  $\sigma$  should be one magnitude smaller, following the anticipated performance of future geodetic VLBI systems (Petrachenko et al., 2009).

---

<sup>1</sup>Other forms of these estimators are also used e.g., in order to discriminate between specific noise types or to provide a better confidence of the resulting stability estimates.

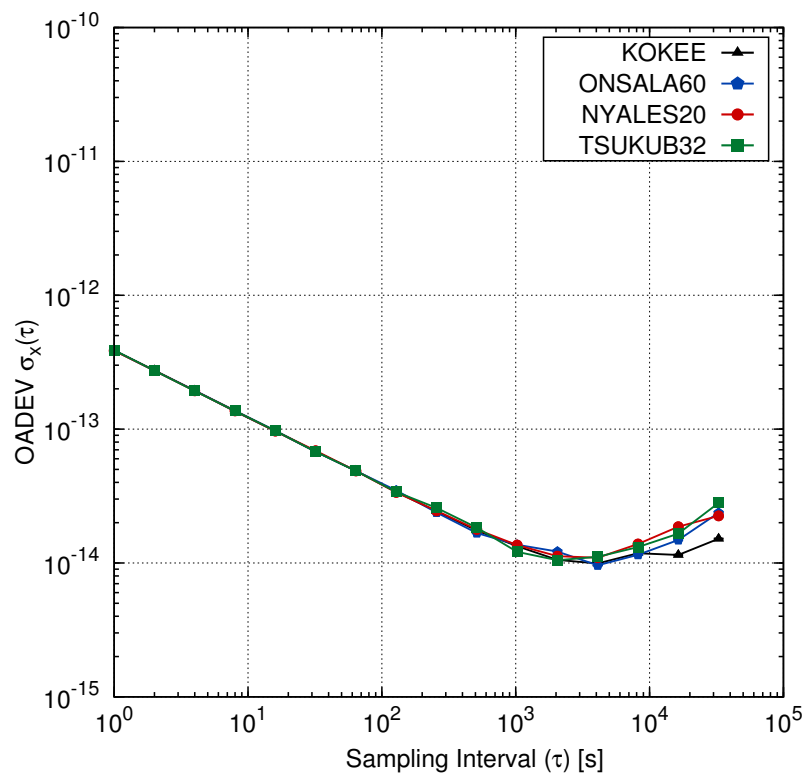


Fig. 4.2: Stability characteristics of four hydrogen masers based on 24 hours of simulated clock data. Parameters of the model:  $1 \cdot 10^{-14}$ @3000 s, corresponding to the current performance of the VLBI maser systems.



## LUNAR OBSERVATIONS WITH GEODETIC VLBI

The VLBI technique can also be used for observations of spacecrafts (Lebreton et al., 2005; Duev et al., 2012). Besides of navigation purposes, such near-field observations can be utilized as an input to planetary orbit determination (Jones et al., 2015) and to bind planetary ephemerids to the ICRF. The differential VLBI technique ( $\Delta$ VLBI) is used for measuring the angular position of the target sources w.r.t a nearby calibrator source.  $\Delta$ VLBI is directly related to the absolute change in phase while canceling out the ionospheric and tropospheric contributions. It provides an increased precision compared to geodetic VLBI, in which group delay observables are used (Takahashi et al., 2000).

Few experiments have also been carried out regarding determination of the relative and absolute position of lunar landers and lunar satellites with VLBI (King et al., 1976). Recent exploration projects such as the LADEE (Lunar Atmosphere and Dust Environment Explorer), CLEP (Chinese Lunar Exploration Program) or GRAIL (Gravity Recovery and Interior Laboratory) contributed to the research on the lunar atmosphere, geomorphological structure of the outer layer of the Moon or provided new models describing the lunar gravity field (Elphic et al., 2014; Li et al., 2015; Konopliv et al., 2013). During the SELENE (SELenological and ENgineering Explorer) mission (Kato et al., 2008), same-beam phase differential VLBI was used for spacecraft orbit determination, providing data that improved the solution of orbits of the sub-satellites (Kikuchi et al., 2009). Based on the results from the Chang'E-3 (CE-3) mission (Li et al., 2015), it was shown that, with several hours of VLBI observations,  $\Delta$ VLBI can provide the relative position of the rover w.r.t. the lander with meter level precision (Zhou et al., 2015).

Simulation studies concerning determination of the position of a lunar lander have also been made by Wei et al. (2013) or Li et al. (2016). However, the

emphasis in most of the studies is only put on the relative positioning of rovers w.r.t. landers or on the difference between two objects on the Moon (Hanada et al., 1993). Studies of absolute VLBI positioning usually do not include investigations concerning the Earth-based parameters, because they often focus on the benefits for navigation (Huang et al., 2012).

## 5.1 Geodetic VLBI narrowband observations

The geodetic VLBI community has been increasing its interest in observations of artificial radio sources. During the last years a few dedicated geodetic VLBI experiments have been carried out with the purpose to track GNSS satellites (Tornatore et al., 2014; Plank et al., 2017). It is expected that simultaneous multi-technique observations of satellites equipped with space-geodetic equipment (VLBI transmitters, GNSS transmitters and receivers, SLR reflectors) will lead to the improvement of the ITRF and contribute to the integrity of measurements carried out using different space-geodetic techniques. Currently, such co-location satellite projects are in pre-study phases and only a few experimental sessions have been performed so far (Tang et al., 2016). A similar concept of multi-technique measurements could be also applied to the studies of the Moon. A lunar lander equipped with space-geodetic appliances such as LLR reflectors and multi-frequency broadband transmitters would be an unique opportunity for comprehensive investigations concerning the structure and rotation of the Moon and dynamics of the Earth-Moon system.

During the Chang'E-3 (CE-3) mission, a robotic lander and a rover were deployed to the lunar surface in late 2013. Its main scientific objectives included the examination of the geological structure of the Moon and visible/near-infrared observations of celestial bodies. In April 2014 first observations of CE-3 signals (at X-band frequencies) with geodetic VLBI telescopes were carried out (Klopotek et al., 2017). The IVS Observing Program Committee agreed also to schedule sessions in which this lander would be observed more often and with a global network of IVS stations. As a result, twelve OCEL sessions (Observing the Chang'E Lander with VLBI) were granted by the IVS Observing Program Committee between 2014 and 2016 (Haas et al., 2017).

### 5.1.1 Precision of lunar geodetic VLBI observables

As mentioned in Sec. 3.3, the precision of group delay observables depends on the SNR of the recorded signals and the effective spanned bandwidth. X-band signals of the CE-3 probe include multiple tones, which are separated by a few tens of MHz. As stated by Zheng et al. (2014), this leads to an effective bandwidth of 38.4 MHz. In addition, assuming acquisition of signals with SNR

values of at least 1000<sup>1</sup>, VLBI group delays could be obtained with a precision on the order of few picoseconds.

Although the theoretical precision may look promising, one needs to consider additional noise contributions and the fact that utilization of single-frequency lunar observations poses a problem in mitigation of dispersive delays caused by the ionosphere of the Earth. The simplest solution would be observations of multi-band signals emitted by artificial radio sources on the lunar surface. Dual-frequency narrow bandwidth signals have already been used in lunar studies e.g., during the aforementioned SELENE mission (Wang et al., 2015). In the case of X-band only observations, ionospheric corrections could be obtained from Global Ionospheric Maps (GIM) (Schaer et al., 1996). GIM datasets contain estimates of the Vertical Total Electron Content (VTEC) and are computed every two hours on a  $2.5^\circ \times 5^\circ$  grid in geographic latitude and longitude<sup>2</sup>. The GIM model could provide ionospheric delay corrections on the order of few TECUs accuracy ( $1 \text{ TECU} = 10^{16} \text{ electrons} / \text{m}^2$ ). Therefore, for the X-band observations, intercontinental baselines and moderate target elevation angles ( $\varepsilon \approx 20^\circ$ ), the residual ionospheric error is expected to be on the level of 0.2 ns, which corresponds to an uncertainty of about 60 mm. This quantity tends to be much smaller on shorter baselines (Ros et al., 2000; Sekido et al., 2003; Hobiger et al., 2006).

## 5.2 BCRS position of an object on the Moon

If one considers an artificial source located on the surface of a planet, there is the necessity of transforming its position from the body-fixed system to the BCRS in order to compute the VLBI near-field delay. This can be done using planetary and lunar ephemeris data such as the Jet Propulsion Laboratory Development Ephemeris (JPL DE) (Folkner et al., 2009) and following several coordinate transformations. First, one needs to convert the position of the object (L) from the body (PA) to the space-fixed system (ICRS), defined relative to the center of mass of a given body (B)

$$\vec{\mathbf{r}}_L^{ICRS} = \mathbf{A}^{ICRS} \vec{\mathbf{r}}_L^{PA}, \quad (5.1)$$

in which  $\vec{\mathbf{r}}_L$  is the position vector of the object in cartesian coordinates and  $\mathbf{A}^{ICRS}$  is the transformation matrix from the body-fixed (Principal Axes of inertia) to the ICRS. If the initial system is the Mean Earth (ME), the ME-PA transformation involves small ephemeris-specific system rotations, which are usually on the arc-second level. The JPL DE ephemerides contain the values of lunar librations, which provide the orientation of the PA system relative to the ICRS

<sup>1</sup>a very conservative assumption compared to the actual results (Klopotek et al., 2017)

<sup>2</sup>[www.igs.org/products](http://www.igs.org/products)

Earth equator and equinox. Therefore, the  $\mathbf{A}^{ICRS}$  matrix can be expressed as the product of three coordinate system rotations

$$\mathbf{A}_{3 \times 3}^{ICRS} = \mathbf{R}_3(-\phi)\mathbf{R}_1(-\omega)\mathbf{R}_3(-\psi), \quad (5.2)$$

where  $\mathbf{R}_1$  and  $\mathbf{R}_3$  are the rotation matrices about the X and Z axes of the right-handed set of axes, respectively. The quantities  $\phi$ ,  $\omega$  and  $\psi$  are the Euler angles describing the orientation of the PA system w.r.t. the ICRS (Archinal et al., 2011). The remaining elements of the object's state vector (velocity, acceleration) are obtained by calculating the first and second order derivatives of  $\mathbf{A}_{3 \times 3}^{ICRS}$  with respect to the  $\phi$ ,  $\omega$  and  $\psi$  angles. Once these values are acquired, the Lorentz transformation is applied in order to express the state vector of an object in the BCRS (Moyer, 2000; Duev et al., 2012).

# Chapter 6

## SUMMARY AND OUTLOOK

The space-time reference frame realized through VLBI provides the basis for global-scale and local-scale measurements in many fields of science. The future challenges for VLBI are mainly related to the realization of the VGOS concept. With the continuous advances in hardware, software and with an increasing number of VGOS stations, it should be possible to decrease the measurement noise-floor, improve the station position accuracy and precision as well as provide high-quality EOPs with an unprecedented level of quality. Combination of other technologies, multidisciplinary approaches and the development of new observing concepts are necessary in order to fully benefit from the opportunities emerging from the continuous operations in the VGOS era. Further research is also required for collocation of space-geodetic techniques in space in order to improve the ITRF and advance our understanding of the processes that are causing the Earth system to change.

The next-generation VLBI system could include a radio transmitter on the Moon and thus complement LLR, reducing systematic errors and providing a measurement sensitivity in the direction perpendicular to the line-of-sight. Long-term and frequent lunar VLBI observations could be of interest for routine observing programs coordinated by the IVS. Within the same 24-hour experiments or during continuous VGOS operations a global network of VLBI stations could track lunar transmitters as well as carry out quasar observations. On the contrary, care has to be taken when new observation types are considered. In case they are scheduled, the near-field observations should not negatively impact the Earth-based parameters. Therefore, optimized and dedicated observing sessions need to be studied in more detail in order to draw conclusions concerning benefits of lunar observations for studies of the Earth-Moon dynamics, rotational properties of the Moon and determination of the classical geodetic parameters. The future work could also include geodetic analysis of real lunar observations and further development of the utilized software. The simulation

studies concerning observations of lunar radio sources and UT1-UTC determination are expected to contribute to a better understanding of dynamic Earth processes and stimulate new observing concepts for GGOS.

## 6.1 Summary of Paper I

### *Geodetic VLBI with an artificial radio source on the Moon: A simulation study*

In the first contribution the concept of geodetic VLBI observations to an artificial radio source on the surface of the Moon was investigated through extensive Monte Carlo simulations using the *c5++* analysis software. The simulation runs were based on networks and settings reflecting the present VLBI and future VGOS performance. It was described how the quality and quantity of lunar observations affect the determination of the lunar lander's position and classical geodetic parameters (station positions, EOPs). The limiting factors of the concept and deficiencies of the study were also revealed.

The determination of the position of an artificial radio source on the Moon with the current VLBI system could be achieved with a submeter precision. Based on the simulations reflecting the future VGOS performance, the accuracy of the horizontal position components would be better than 5 cm, assuming ionosphere-free observables. The inclusion of lunar observations into IVS-R1 schedules did not negatively impact the estimation of EOPs and coordinates of the VLBI stations.

## 6.2 Summary of Paper II

### *Identifying optimal tag-along station locations for improving VLBI Intensive sessions*

The one-hour VLBI intensive sessions (INT1, INT2, INT3) are carried out in order to provide daily UT1-UTC estimates. In the case of INT1 and INT2 sessions, the observing network consists of two VLBI stations. In this paper, the possibility to enhance the UT1-UTC determination by including a third VLBI telescope to the INT1 and INT2 observing networks in a tag-along mode was investigated. This was studied through Monte Carlo simulations using the *c5++* analysis software. It was shown that the inclusion of an additional station would provide UT1-UTC estimates with up to 40 % smaller yearly WRMS, compared to simulations relying on a single-baseline approach.

### 6.3 Summary of Paper III

#### *Implementation of VLBI Near-Field Delay Models in the c5++ Analysis Software*

The implementation of two VLBI near-field delay models by Sekido and Fukushima (2006) and Duev et al. (2012) in the *c5++* analysis software is described and the models themselves are compared. The latter was carried out using near-field delays computed for four baselines (one European and three intercontinental) over a period of 30 days. The differences between the delays from both models tend to scale with the distance between the stations and can amount up to 300 ps at some epochs for intercontinental baselines.

Correlation results from test observations to the lander on the ONSALA60–WETTZELL baseline are also presented in this paper. *c5++* was included in the processing chain in order to obtain a priori delay information, which is crucial in correlation of the VLBI raw observations of the Chang'E-3 lander.

### 6.4 Summary of Paper IV

#### *Results from the VLBI Analysis Software Comparison Campaign 2015*

The aim of the VLBI Analysis Software Comparison Campaign 2015 (VASCC2015) was to compare different VLBI analysis software packages on the basis of computed theoretical delays using two different test networks during a period of 15 days. The project included packages which are used for operational VLBI analysis as well as those which are still under development. During the VASCC2015, numerical issues were identified and several bugs could be fixed in some of the softwares. The results indicate that a sub-millimeter agreement of theoretical delays, computed by state-of-the-art VLBI analysis software packages, can be achieved.



# BIBLIOGRAPHY

- Agnew, D.C., 2007. Earth Tides, in: Herring, T.A. (Ed.), *Treatise on Geophysics: Geodesy*, Elsevier, New York. pp. 163–195.
- Altamimi, Z., Rebischung, P., Métivier, L., Collilieux, X., 2016. ITRF2014: A new release of the International Terrestrial Reference Frame modeling nonlinear station motions. *Journal of Geophysical Research: Solid Earth* doi:10.1002/2016JB013098.
- Archinal, B.A., A’Hearn, M.F., Bowell, E., Conrad, A., Consolmagno, G.J., Courtin, R., Fukushima, T., Hestroffer, D., Hilton, J.L., Krasinsky, G.A., Neumann, G., Oberst, J., Seidelmann, P.K., Stooke, P., Tholen, D.J., Thomas, P.C., Williams, I.P., 2011. Report of the IAU Working Group on Cartographic Coordinates and Rotational Elements: 2009. *Celestial Mechanics and Dynamical Astronomy* 109, 101–135. doi:10.1007/s10569-010-9320-4.
- Azouit, M., Vernin, J., 2005. Optical Turbulence Profiling with Balloons Relevant to Astronomy and Atmospheric Physics. *Publications of the Astronomical Society of the Pacific* 117, 536. doi:10.1086/429785.
- Bachmann, S., Thaller, D., Roggenbuck, O., Lösler, M., Messerschmitt, L., 2016. IVS contribution to ITRF2014. *Journal of Geodesy* 90, 631–654. doi:10.1007/s00190-016-0899-4.
- Behrend, D., Cucurull, L., Vilà, J., Haas, R., 2000. An inter-comparison study to estimate zenith wet delays using VLBI, GPS, and NWP models. *Earth, Planets and Space* 52, 691–694. doi:10.1186/BF03352265.
- Böhm, J., Niell, A., Tregoning, P., Schuh, H., 2006. Global Mapping Function (GMF): A new empirical mapping function based on numerical weather model data. *Geophysical Research Letters* 33. doi:10.1029/2005GL025546.
- Bolotin, S., Baver, K., Gipson, J., Gordon, D., MacMillan, D., 2014. The VLBI Data Analysis Software  $\nu$ Solve: Development Progress and Plans for the Fu-

- ture, in: Baver, K.D., Behrend, D., Armstrong, K.L. (Eds.), *IVS 2014 General Meeting Proceedings*, Science Press, Beijing. pp. 253–257.
- Born, M., Wolf, E., 1970. *Principles of Optics*. Fourth ed., Pergamon Press Inc., Bath.
- Capitaine, N., Guinot, B., McCarthy, D.D., 2000. Definition of the Celestial Ephemeris Origin and of UT1 in the International Celestial Reference Frame. *Astronomy and Astrophysics* 335, 398–405.
- Capitaine, N., Wallace, P.T., Chapront, J., 2003. Expressions for IAU 2000 precession quantities. *Astronomy and Astrophysics* 412, 567–586. doi:10.1051/0004-6361:20031539.
- Cappallo, R., 2014. Correlating and Fringe-fitting Broadband VGOS Data, in: Behrend, D., Baver, K.D., Armstrong, K.L. (Eds.), *IVS 2014 General Meeting Proceedings*, International VLBI Service for Geodesy and Astrometry. pp. 91–96.
- Chao, B.F., Dong, D.N., Liu, H.S., Herring, T.A., 1991. Libration in the Earth's rotation. *Geophysical Research Letters* 18, 2007–2010. doi:10.1029/91GL02491.
- Davis, J.L., Herring, T.A., Shapiro, I.I., Rogers, A.E.E., Elgered, G., 1985. Geodesy by radio interferometry: Effects of atmospheric modeling errors on estimates of baseline length. *Radio Science* 20, 1593–1607. doi:10.1029/RS020i006p01593.
- Deller, A.T., Tingay, S., Bailes, M., West, C., 2007. DiFX: A Software Correlator for Very Long Baseline Interferometry Using Multi-processor Computing Environments. *Publications of the Astronomical Society of the Pacific* 119, 318–336. doi:dx.doi.org/10.1086/513572.
- Desai, S.D., 2002. Observing the pole tide with satellite altimetry. *Journal of Geophysical Research: Oceans* 107, 7–1–7–13. doi:10.1029/2001JC001224.
- Duev, D.A., Calves, Molera, G., Pogrebenko, S.V., Gurvits, L.I., Cimo, G., Bahamon, T.B., 2012. Spacecraft VLBI and doppler tracking: algorithms and implementation. *Astronomy & Astrophysics* 541, A43. doi:10.1051/0004-6361/201218885.
- Elphic, R.C., Delory, G.T., Hine, B.P., Mahaffy, P.R., Horanyi, M., Colaprete, A., Benna, M., Noble, S.K., 2014. The Lunar Atmosphere and Dust Environment Explorer Mission. *Space Science Reviews* 185, 3–25. doi:10.1007/s11214-014-0113-z.

- Fey, A.L., Gordon, D., Jacobs, C.S. (Eds.), 2009. The Second Realization of the International Celestial Reference Frame by Very Long Baseline Interferometry, Presented on behalf of the IERS / IVS Working Group. IERS Technical Note 35, Verlag des Bundesamts für Kartographie und Geodäsie, Frankfurt am Main.
- Folkner, W.M., Williams, J.G., Boggs, D.H., 2009. The Planetary and Lunar Ephemeris DE 421. IPN Progress Report 42-178.
- Gipson, J., 2012. IVS Working Group 4: VLBI Data Structures, in: Behrend, D., Baver, K.D. (Eds.), *IVS 2012 General Meeting Proceedings*, International VLBI Service for Geodesy and Astrometry. pp. 212–221.
- Gipson, J., 2014. IVS Working Group IV and the New Open Format Database, in: Behrend, D., Baver, K.D., Armstrong, K.L. (Eds.), *IVS 2014 General Meeting Proceedings*, International VLBI Service for Geodesy and Astrometry. pp. 248–252.
- Haas, R., Halsig, S., Han, S., Iddink, A., Jaron, F., La Porta, L., Lovell, J., Neidhardt, A., Nothnagel, A., Plötz, C., Tang, G., Zhang, Z., 2017. Observing the Chang'E-3 Lander with VLBI (OCEL): Technical Setups and First Results, in: Nothnagel, A., Jaron, F. (Eds.), *Proceedings of the First International Workshop on VLBI Observations of Near-field Targets, October 5 - 6, 2016*, Schriftenreihe des Inst. f. Geodäsie u. Geoinformation, Vol. 54, ISSN 1864-1113, Bonn. pp. 41–64.
- Haas, R., Schuh, H., 1996. Determination of frequency dependent Love and Shida numbers from VLBI data. *Geophysical Research Letters* 23, 1509–1512. doi:10.1029/96GL00903.
- Halsig, S., Artz, T., Iddink, A., Nothnagel, A., 2016. Using an atmospheric turbulence model for the stochastic model of geodetic VLBI data analysis. *Earth, Planets and Space* 68, 1–14. doi:10.1186/s40623-016-0482-5. b03407.
- Hanada, H., Ooe, M., Kawaguchi, N., Kawano, N., Kuji, S., Sasao, T., Tsuruta, S., Fujishita, M., Morimoto, M., 1993. Study of the Lunar Core by VLBI Observations of Artificial Radio Sources on the Moon. *Journal of Geomagnetism and Geoelectricity* 45, 1405–1414. doi:10.5636/jgg.45.1405.
- Hawarey, M., Hobiger, T., Schuh, H., 2005. Effects of the 2nd order ionospheric terms on VLBI measurements. *Geophysical Research Letters* 32. doi:10.1029/2005GL022729. 111304.
- Herring, T.A., 1992. Submillimeter Horizontal Position Determination Using Very Long Baseline Interferometry. *Journal of Geophysical Research: Solid Earth* 97, 1981–1990. doi:10.1029/91JB02649.

- Herring, T.A., Davis, J.L., Shapiro, I.I., 1990. Geodesy by radio interferometry: The application of Kalman Filtering to the analysis of very long baseline interferometry data. *Journal of Geophysical Research: Solid Earth* 95, 12561–12581. doi:10.1029/JB095iB08p12561.
- Himwich, E., 2000. Introduction to the Field System for Non-Users, in: Vandenberg, N.R., Baver, K.D. (Eds.), *IVS 2000 General Meeting Proceedings*, International VLBI Service for Geodesy and Astrometry. pp. 86–90.
- Hobiger, T., Ichikawa, R., Koyama, Y., Kondo, T., 2008. Fast and accurate ray-tracing algorithms for real-time space geodetic applications using numerical weather models. *Journal of Geophysical Research: Atmospheres* 113. doi:10.1029/2008JD010503.
- Hobiger, T., Kondo, T., Schuh, H., 2006. Very Long Baseline Interferometry as a tool to probe the ionosphere. *Radio Science* 41. doi:10.1029/2005RS003297.
- Hobiger, T., Otsubo, T., 2014. Combination of GPS and VLBI on the observation level during CONT11—common parameters, ties and inter-technique biases. *Journal of Geodesy* 88, 1017–1028. doi:10.1007/s00190-014-0740-x.
- Hobiger, T., Otsubo, T., Sekido, M., Gotoh, T., Kubooka, T., Takiguchi, H., 2010. Fully automated VLBI analysis with c5++ for ultra rapid determination of ut1. *Earth Planets Space* 62, 933–937. doi:10.5047/eps.2010.11.008.
- Hofmeister, A., Böhm, J., 2017. Application of ray-traced tropospheric slant delays to geodetic VLBI analysis. *Journal of Geodesy* , 1–20.
- Howe, D.A., Allan, D.W., Barnes, J.A., 1981. Properties of Signal Sources and Measurement Methods, in: *Proceedings of the 35th Annual Symposium on Frequency Control*, Defense Technical Information Center. pp. 464–469.
- Huang, Y., Hu, X., Li, P., Cao, J., Jiang, D., Zheng, W., Fan, M., 2012. Precise positioning of the Chang'E-3 lunar lander using a kinematic statistical method. *Chinese Science Bulletin* 57, 4545–4551. doi:10.1007/s11434-012-5484-5.
- Jones, D.L., Folkner, W.M., Jacobson, R.A., Jacobs, C.S., Dhawan, V., Romney, J., Fomalont, E., 2015. Astrometry of Cassini With the VLBA to Improve the Saturn Ephemeris. *Astronomical Journal* 149, 28. doi:10.1088/0004-6256/149/1/28.
- Kareinen, N., Hobiger, T., Haas, R., 2015. Automated analysis of Kokee–Wettzell Intensive VLBI sessions—algorithms, results, and recommendations. *Earth, Planets and Space* 67, 1–13. doi:10.1186/s40623-015-0340-x.

- Kareinen, N., Hobiger, T., Haas, R., 2016. Automated ambiguity estimation for VLBI Intensive sessions using L1-norm. *Journal of Geodynamics* 102, 39 – 46. doi:<https://doi.org/10.1016/j.jog.2016.07.003>.
- Kato, M., Sasaki, S., Tanaka, K., Iijima, Y., Takizawa, Y., 2008. The Japanese lunar mission SELENE: Science goals and present status. *Advances in Space Research* 42, 294–300. doi:10.1016/j.asr.2007.03.049.
- Kikuchi, F., Liu, Q., Hanada, H., Kawano, N., Matsumoto, K., Iwata, T., Goossens, S.J., Asari, K., Ishihara, Y., Tsuruta, S., Ishikawa, T., Noda, H., Namiki, N., Petrova, N., Harada, Y., Ping, J., Sasaki, S., 2009. Picosecond accuracy VLBI of the two subsatellites of SELENE (KAGUYA) using multifrequency and same beam methods. *Radio Science* 44. doi:10.1029/2008RS003997.
- King, R.W., Counselman, C.C., Shapiro, I.I., 1976. Lunar dynamics and selenodesy: Results from analysis of VLBI and laser data. *Journal of Geophysical Research* 81, 6251–6256. doi:10.1029/JB081i035p06251.
- Klioner, S.A., 2003. A Practical Relativistic Model for Microarcsecond Astrometry in Space. *The Astronomical Journal* 125, 1580. doi:10.1086/367593.
- Klopotek, G., Hobiger, T., Haas, R., 2017. Implementation of VLBI Near-Field Delay Models in the c5++ Analysis Software, in: Nothnagel, A., Jaron, F. (Eds.), *Proceedings of the First International Workshop on VLBI Observations of Near-field Targets, October 5 - 6, 2016*, Schriftenreihe des Inst. f. Geodäsie u. Geoinformation, Vol. 54, ISSN 1864-1113, Bonn. pp. 29–33.
- Konopliv, A.S., Park, R.S., Yuan, D.N., Asmar, S.W., Watkins, M.M., Williams, J.G., Fahnestock, E., Kruizinga, G., Paik, M., Strelakov, D., Harvey, N., Smith, D.E., Zuber, M.T., 2013. The jpl lunar gravity field to spherical harmonic degree 660 from the grail primary mission. *Journal of Geophysical Research: Planets* 118, 1415–1434. doi:10.1002/jgre.20097.
- Kudryavtsev, S.M., 2004. Improved harmonic development of the Earth tide-generating potential. *Journal of Geodesy* 77, 829–838. doi:10.1007/s00190-003-0361-2.
- Lebreton, J.P., Witasse, O., Sollazzo, C., Blancquaert, T., Couzin, P., Schipper, A.M., Jones, J.B., Matson, D.L., Gurvits, L.I., Atkinson, D.H., Kazeminejad, B., Perez-Ayucar, M., 2005. An overview of the descent and landing of the Huygens probe on Titan. *Nature* 438, 758–764. doi:10.1038/nature04347.
- Li, C., Liu, J., Ren, X., Zuo, W., Tan, X., Wen, W., Li, H., Mu, L., Su, Y., Zhang, H., Yan, J., Ouyang, Z., 2015. The Chang'e 3 Mission Overview. *Space Science Reviews* 190, 85–101. doi:10.1007/s11214-014-0134-7.

- Li, F., Ye, M., Yan, J., Hao, W., Barriot, J.P., 2016. A simulation of the Four-way lunar Lander-Orbiter tracking mode for the Chang'E-5 mission. *Advances in Space Research* 57, 2376 – 2384. doi:10.1016/j.asr.2016.03.007.
- Ma, C., Arias, E.F., Eubanks, T.M., Fey, A.L., Gontier, A.M., Jacobs, C.S., Sovers, O.J., Archinal, B.A., Charlot, P., 1998. The International Celestial Reference Frame as Realized by Very Long Baseline Interferometry. *The Astronomical Journal* 116, 516.
- Ma, C., Sauber J.M., Bell L.J., Clark, T., Gordon, D., Himwich W.E., Ryan J.W., 1990. Measurement of horizontal motions in Alaska using very long baseline interferometry. *Journal of Geophysical Research: Solid Earth* 95, 21991–22011. doi:10.1029/JB095iB13p21991.
- MacMillan, D.S., 1995. Atmospheric gradients from very long baseline interferometry observations. *Geophysical Research Letters* 22, 1041–1044. doi:10.1029/95GL00887.
- Malkin, Z., Jacobs, C.S., Arias, E.F., Boboltz, D., Böhm, J., Bolotin, S., Bourda, G., Charlot, P., De Witt, A., Fey, A.L., Gaume, R., Heinkelmann, R., Lambert, S., Ma, C., Nothnagel, A., Seitz, D., Gordon, D., Skurikhina, E., Souchay, J., Titov, O., 2015. The ICRF-3: Status, plans, and progress on the next generation International Celestial Reference Frame, in: Malkin, Z., Capitaine, N. (Eds.), *Proceedings of the Journées 2014 "Systèmes de référence Spatio-temporels" (JSR2014)*, pp. 3–8.
- Mathews, P.M., Buffett, B.A., Shapiro, I.I., 1995. Love numbers for diurnal tides: Relation to wobble admittances and resonance expansions. *Journal of Geophysical Research: Solid Earth* 100, 9935–9948. doi:10.1029/95JB00670.
- Mathews, P.M., Herring, T.A., Buffett, B.A., 2002. Modeling of nutation and precession: New nutation series for nonrigid Earth and insights into the Earth's interior. *Journal of Geophysical Research: Solid Earth* 107, ETG 3–1–ETG 3–26. doi:10.1029/2001JB000390.
- Moyer, T.D., 2000. Formulation for Observed and Computed Values of Deep Space Network Data Types for Navigation. JPL Deep-Space Communications and Navigation Series.
- Niell, A., 1996. Global mapping functions for the atmosphere delay at radio wavelengths. *Journal of Geophysical Research: Solid Earth* 101, 3227–3246. doi:10.1029/95JB03048.
- Niell, A., Beaudoin, C.J., Bolotin, S., Cappallo, R.J., Corey, B.E., Gipson, J., Gordon, D., McWhirter, R., Ruzsarczyk, C.A., SooHoo, J., 2014. VGOS Operations and Geodetic Results, in: Behrend, D., Baver, K.D., Armstrong, K.L. (Eds.),

- IVS 2014 General Meeting Proceedings*, International VLBI Service for Geodesy and Astrometry. pp. 97–101.
- Niell, A., Whitney, A., Petrachenko, B., Schlüter, W., Vandenberg, N., Hase, H., Koyama, Y., Ma, C., Schuh, H., Tuccari, G., 2005. VLBI2010: Current and Future Requirements for Geodetic VLBI Systems, in: Behrend, D., Baver, K. (Eds.), *International VLBI Service for Geodesy and Astrometry 2005 Annual Report*, IVS Coordinating Center.
- Nilsson, T., Davis, J.L., Hill, E.M., 2009. Using ground-based GPS to characterize atmospheric turbulence. *Geophysical Research Letters* 36. doi:10.1029/2009GL040090.116807.
- Nilsson, T., Gradinarsky, L., Elgered, G., 2005. Correlations Between Slant Wet Delays Measured by Microwave Radiometry. *IEEE Transactions on Geoscience and Remote Sensing* 43, 1028–1035.
- Nilsson, T., Haas, R., 2010. Impact of atmospheric turbulence on geodetic very long baseline interferometry. *Journal of Geophysical Research: Solid Earth* 115. doi:10.1029/2009JB006579.
- Nilsson, T., Haas, R., Elgered, G., 2007. Simulations of Atmospheric Path Delays Using Turbulence Models, in: Böhm, J., Pany, A., Schuh, H. (Eds.), *Proceedings of the 18th Working Meeting on European VLBI for Geodesy and Astrometry*, Geowissenschaftliche Mitteilungen, Schriftenreihe der Studienrichtung Vermessung und Geoinformation, Technische Universität Wien. pp. 175–180.
- Nothnagel, A., 2009. Conventions on thermal expansion modelling of radio telescopes for geodetic and astrometric VLBI. *Journal of Geodesy* 83, 787–792. doi:10.1007/s00190-008-0284-z.
- Nothnagel, A., Artz, T., Behrend, D., Malkin, Z., 2016. International VLBI Service for Geodesy and Astrometry - Delivering high-quality products and embarking on observations of the next generation. *Journal of Geodesy* .
- Nothnagel, A., Schnell, D., 2008. The impact of errors in polar motion and nutation on UT1 determinations from VLBI Intensive observations. *Journal of Geodesy* 82, 863–869. doi:10.1007/s00190-008-0212-2.
- Petit, G., Luzum, B. (Eds.), 2010. IERS Conventions (2010). IERS Technical Note 36, Verlag des Bundesamts für Kartographie und Geodäsie, Frankfurt am Main.
- Petrachenko, B., Niell, A., Behrend, D., Corey, B., Böhm, J., Charlot, P., Collioud, A., Gipson, J., Haas, R., Hobiger, T., Koyama, Y., MacMillan, D., Malkin, Z.,

- Nilsson, T., Pany, A., Tuccari, G., Whitney, A., Wresnik, J., 2009. Design aspects of the VLBI2010 system. Progress Report of the IVS VLBI2010 Committee .
- Plag, H.P., Pearlman, M. (Eds.), 2009. Global Geodetic Observing System: Meeting the Requirements of a Global Society on a Changing Planet in 2020. First ed., Springer-Verlag Berlin Heidelberg. doi:10.1007/978-3-642-02687-4.
- Plank, L., Hellerschmied, A., McCallum, J., Böhm, J., Lovell, J., 2017. VLBI observations of GNSS-satellites: from scheduling to analysis. *Journal of Geodesy* 91, 1–14.
- Rao, D.N., Rao, T.N., Venkataratnam, M., Thulasiraman, S., Rao, S.V.B., Srinivasulu, P., Rao, P.B., 2001. Diurnal and seasonal variability of turbulence parameters observed with Indian mesosphere-stratosphere-troposphere radar. *Radio Science* 36, 1439–1457. doi:10.1029/2000RS002316.
- Ray, R.D., Ponte, R.M., 2003. Barometric tides from ECMWF operational analyses. *Annales Geophysicae* 21, 1897–1910. doi:10.5194/angeo-21-1897-2003.
- Rogers, A.E.E., 1970. Very Long Baseline Interferometry with Large Effective Bandwidth for Phase-Delay Measurements. *Radio Science* 5, 1239–1247. doi:10.1029/RS005i010p01239.
- Ros, E., Marcaide, J.M., Guirado, J.C., Sardón, E., Shapiro, I.I., 2000. A GPS-based method to model the plasma effects in VLBI observations. *Astronomy & Astrophysics* 356, 357–362.
- Salminen, T., 2015. Flexible and transparent buffering of radio astronomy measurements: VLBI-streamer and Flexbuff. Master's thesis. Aalto University.
- Schaer, S., Beutler, G., Rothacher, M., Springer, T.A., 1996. Daily global ionosphere maps based on GPS carrier phase data routinely produced by the CODE, in: Neilan, R.E., Van Scoy, P.A., Zumberge, J.F. (Eds.), *Proceedings of the IGS Analysis Center Workshop*, International GNSS Service.
- Scherneck, H.G., 2016. Loading Effects, in: Grafarend, E. (Ed.), *Encyclopedia of Geodesy*, Springer International Publishing, Cham. pp. 1–12. doi:10.1007/978-3-319-02370-0\_52-1.
- Sekido, M., Fukushima, T., 2006. A VLBI Delay Model for Radio Sources at a Finite Distance. *Journal of Geodesy* 80, 137–149. doi:10.1007/s00190-006-0035-y.
- Sekido, M., Kondo, T., Kawai, E., Imae, M., 2003. Evaluation of GPS-based ionospheric TEC map by comparing with VLBI data. *Radio Science* 38. doi:10.1029/2000RS002620.

- Shaffer, D.B., 2000. RFI: Effects on Bandwidth Synthesis, in: Vandenberg, N.R., Baver, K.D. (Eds.), *IVS 2000 General Meeting Proceedings*, International VLBI Service for Geodesy and Astrometry. pp. 402–406.
- da Silva Neto, D.N., Andrei, A.H., Vieira Martins, R., Assafin, M., 2002. A Pattern of Noncoincidence between Radio and Optical Positions of International Celestial Reference Frame Sources. *The Astronomical Journal* 124, 612.
- Sovers, O.J., Fanselow, J.L., Jacobs, C.S., 1998. Astrometry and geodesy with radio interferometry: experiments, models, results. *Reviews of Modern Physics* 70, 1393–1454. doi:10.1103/RevModPhys.70.1393.
- Takahashi, F., Kondo, T., Takahashi, Y., Koyama, Y., 2000. Very Long Baseline Interferometer. Wave summit course, *Ohmsha*, Ltd.
- Tamura, Y., 1987. A Harmonic Development of the Tide-Generating Potential. *Bulletin d'Informations Marées Terrestres* 99, Bruxelles.
- Tang, G., Sun, J., Li, X., Liu, S., Chen, G., Ren, T., Wang, G., 2016. APOD Mission Status and Observations by VLBI, in: Behrend, D., Baver, K.D., Armstrong, K.L. (Eds.), *IVS 2016 General Meeting Proceedings*, International VLBI Service for Geodesy and Astrometry. pp. 363–367.
- Tatarskii, V.I., 1971. The effects of the turbulent atmosphere on wave propagation. *Israel Program for Scientific Translations*, Jerusalem.
- Titov, O., Tesmer, V., Böhm, J., 2004. OCCAM v.6.0 Software for VLBI Data Analysis, in: Vandenberg, N., Baver, K.D. (Eds.), *IVS 2004 General Meeting Proceedings*, International VLBI Service for Geodesy and Astrometry. pp. 267–271.
- Tornatore, V., Haas, R., Casey, S., Duev, D., Pogrebenko, S.V., Calvés, G.M., 2014. Direct VLBI Observations of Global Navigation Satellite System Signals, in: Rizos, C., Willis, P. (Eds.), *Earth on the Edge: Science for a Sustainable Planet: Proceedings of the IAG General Assembly*, Springer Berlin Heidelberg, Berlin, Heidelberg. pp. 247–252. doi:10.1007/978-3-642-37222-3\_32.
- Treuhaft, R.N., Lanyi, G.E., 1987. The effect of the dynamic wet troposphere on radio interferometric measurements. *Radio Science* 22, 251–265. doi:10.1029/RS022i002p00251.
- Tuccari, G., Alef, W., Bertarini, A., Buttaccio, S., Comoretto, G., Graham, D., Neidhardt, A., Platania, P.R., Russo, A., Rov, A., Wunderlich, M., Zeitlhöfler, R., Xaing, Y., 2010. DBBC2 Backend: Status and Development Plan, in: Behrend, D., Baver, K.D. (Eds.), *IVS 2010 General Meeting Proceedings*, International VLBI Service for Geodesy and Astrometry. pp. 392–395.

- Tuccari, G., Alef, W., Buttaccio, S., Casey, S., Felke, A., Lindqvist, M., Wunderlich, M., 2014. DBBC3: An EVN and VGOS All-inclusive VLBI System, in: Behrend, D., Baver, K.D., Armstrong, K.L. (Eds.), *IVS 2014 General Meeting Proceedings*, International VLBI Service for Geodesy and Astrometry. pp. 86–90.
- Tuccari, G., Buttaccio, S., Nicotra, G., Xiang, Y., Michael, W., 2006. DBBC - A Flexible Platform for VLBI Data Processing, in: Behrend, D., Baver, K.D. (Eds.), *IVS 2006 General Meeting Proceedings*, International VLBI Service for Geodesy and Astrometry. pp. 185–189.
- Vasseur, H., 1999. Prediction of tropospheric scintillation on satellite links from radiosonde data. *IEEE Transactions on Antennas and Propagation* 47, 293–301. doi:10.1109/8.761069.
- Wahr, J.M., 1985. Deformation induced by polar motion. *Journal of Geophysical Research: Solid Earth* 90, 9363–9368. doi:10.1029/JB090iB11p09363.
- Wang, Z., Wang, N., Ping, J.S., 2015. Electron content near the lunar surface using dual-frequency VLBI tracking data in a single lunar orbiter mission. *Research in Astronomy and Astrophysics* 15, 753–763. doi:10.1088/1674-4527/15/5/012.
- Wei, E., Jin, S., Yang, H., Li, X., Gu, H., Li, Z., Li, J., Matsumoto, K., Liu, J., 2013. Simulation and results on real-time positioning of Chang'E-3 rover with the same-beam VLBI observations. *Planetary and Space Science* 84, 20–27. doi:10.1016/j.pss.2013.04.005.
- Whitney, A., Lonsdale, C., Himwich, E., Vandenberg, N., van Langevelde, H., Mujunen, A., Walker, C., 2002. VEX File Definition/Example. <http://www.vlbi.org/vex/docs/vex%20definition%2015b1.pdf>. Technical report 1.5b1.
- Whitney, A.R., 2004. The Mark 5B VLBI Data System, in: Vandenberg, N., Baver, K.D. (Eds.), *IVS 2004 General Meeting Proceedings*, International VLBI Service for Geodesy and Astrometry. pp. 177–181.
- Whitney, A.R., Cappallo, R.J., Ruzsczyk, C.A., SooHoo, J., Crew, G.B., 2014. Mark 6 16-Gbps Next-Generation VLBI Data System, in: Behrend, D., Baver, K.D., Armstrong, K.L. (Eds.), *IVS 2014 General Meeting Proceedings*, International VLBI Service for Geodesy and Astrometry. pp. 86–90.
- Wresnik, J., 2009. Simulationen für die neue Generation von VLBI-Systemen. Ph.D. thesis. Vienna University of Technology.
- Zheng, W., Huang, Y., Chen, Z., Wang, G.W., Liu, Q., Tong, F., Li, P., 2014. Realtime and High-Accuracy VLBI in the CE-3 Mission, in: Behrend, D., Baver,

- K.D., Armstrong, K.L. (Eds.), *IVS 2014 General Meeting Proceedings*, International VLBI Service for Geodesy and Astrometry. pp. 466–472.
- Zhou, H., Li, H., Dong, G., 2015. Relative position determination between Chang'E-3 lander and rover using in-beam phase referencing. *Science China Information Sciences* 58, 1–10. doi:10.1007/s11432-015-5363-1.

